

Provided for non-commercial research and education use.  
Not for reproduction, distribution or commercial use.



This article appeared in a journal published by Elsevier. The attached copy is furnished to the author for internal non-commercial research and education use, including for instruction at the authors institution and sharing with colleagues.

Other uses, including reproduction and distribution, or selling or licensing copies, or posting to personal, institutional or third party websites are prohibited.

In most cases authors are permitted to post their version of the article (e.g. in Word or Tex form) to their personal website or institutional repository. Authors requiring further information regarding Elsevier's archiving and manuscript policies are encouraged to visit:

<http://www.elsevier.com/authorsrights>



Contents lists available at ScienceDirect

Electrochimica Acta

journal homepage: [www.elsevier.com/locate/electacta](http://www.elsevier.com/locate/electacta)

## Review

## Ions and water molecules in an electrolyte solution in contact with charged and dipolar surfaces

Ekaterina Gongadze<sup>a</sup>, Aljaž Velikonja<sup>b,c</sup>, Šarka Perutkova<sup>a</sup>, Peter Kramar<sup>b</sup>, Alenka Maček-Lebar<sup>b</sup>, Veronika Kralj-Iglič<sup>d</sup>, Aleš Iglič<sup>a,\*</sup><sup>a</sup> Laboratory of Biophysics, Faculty of Electrical Engineering, University of Ljubljana, Tržaška 25, SI-1000 Ljubljana, Slovenia<sup>b</sup> Laboratory of Biocybernetics, Faculty of Electrical Engineering, University of Ljubljana, Tržaška 25, SI-1000 Ljubljana, Slovenia<sup>c</sup> SMARTEH Research and Development of Electronic Controlling and Regulating Systems, Trg tigrovcev 1, SI-5220 Tolmin, Slovenia<sup>d</sup> Laboratory of Clinical Biophysics, Faculty of Health Studies, University of Ljubljana, Zdravstvena 5, SI-1000 Ljubljana, Slovenia

## ARTICLE INFO

## Article history:

Received 12 May 2013

Received in revised form 17 July 2013

Accepted 18 July 2013

Available online 2 August 2013

## Keywords:

Water molecules

Permittivity

Orientational ordering

Attractive forces

Electric double layer

## ABSTRACT

The electrolyte-charged surface interface is described within the Langevin–Poisson–Boltzmann (LPB) and Langevin–Bikerman models. It is shown that in the saturation regime close to the charged surface, water dipole ordering and depletion of water molecules may result in a strong local decrease of permittivity. Analytical expressions for the space dependence of relative permittivity are derived for both models. The differential capacitance as a function of the surface potential is calculated within the modified Langevin–Bikerman model and compared to the prediction of the classical Gouy–Chapman theory. As an example of the application of the models described, a zwitterionic lipid surface with non-zero dipole moments in contact with an electrolyte solution of monovalent salt ions and water dipoles is studied within the LPB model. An analytical expression for the osmotic pressure of the electrolyte solution between the zwitterionic lipid surface and a charged particle (macroion) is derived. Some of the predictions of the described electric double layer mean-field theoretical considerations are evaluated using the results of a molecular dynamics simulation. At the end a theoretical description of the possible origin of the attractive interactions between like-charged surfaces mediated by charged macroions with distinctive internal charge distribution is given.

© 2013 Elsevier Ltd. All rights reserved.

## Contents

1. Introduction .....	43
2. Energy of a single water molecule within a triangular atomic model .....	44
3. Point-like molecules in an electrolyte solution .....	44
3.1. Modified Langevin–Poisson–Boltzmann equation .....	44
3.2. Langevin–Poisson–Boltzmann equation .....	46
3.3. Limiting Poisson–Boltzmann equation .....	46
3.4. Osmotic pressure .....	46
4. Finite-sized molecules in an electrolyte solution .....	47
4.1. Gongadze–Iglič equation .....	47
4.2. Langevin–Bikerman equation .....	49
4.3. Bikerman equation .....	49
4.4. Limiting Poisson–Boltzmann equation .....	50
4.5. Osmotic pressure .....	50
5. Differential capacitance .....	51
6. Dipolar surface in contact with an electrolyte solution within the modified Langevin–Poisson–Boltzmann model .....	51
6.1. Modified Langevin–Poisson–Boltzmann for a dipolar surface .....	51
6.2. Comparison with MD simulations .....	52

\* Corresponding author. Tel.: +386 1 4768 825; fax: +386 1 4768 850.

E-mail address: [ales.iglic@fe.uni-lj.si](mailto:ales.iglic@fe.uni-lj.si) (A. Iglič).

6.3.	Average lipid dipolar headgroup orientation angle and osmotic pressure .....	54
7.	Attraction between like-charged surfaces mediated by macroions with internal charge distribution .....	54
7.1.	Spheroidal macroions .....	55
7.2.	Spheroidal and rod-like macroions .....	57
8.	Conclusions .....	58
	Acknowledgements .....	59
	References .....	59

## 1. Introduction

In the complex interface between a charged surface and a surrounding electrolyte (Fig. 1), the electric double layer (EDL) plays a crucial role [1–11]. It causes the ions and water molecules to rearrange near the charged surface and thus to screen the electric potential [12–16]. Due to electrostatic forces between the charged surface and the ions in the electrolyte solution, the counterions (ions with a charge of the sign opposite to the charged surface) are accumulated close to the surface and the co-ions (ions with a charge of the same sign as the surface) are depleted from the surface.

Study of the EDL was begun in 1879 by Hermann von Helmholtz who treated the double layer as a simple capacitor, assuming that the surface charge density is neutralized by the counterions located at a distance equal to their hydrated radius. Gouy [17] and Chapman [18] considered the thermal motion of ions and pictured a diffuse double layer composed of counterions and co-ions. Within the so-called Poisson–Boltzmann (PB) theory [6,12,13,17–20], the ions in electrolyte solution are treated as dimensionless, the surfaces are considered as uniformly charged and uniform permittivity of the electrolyte solution is assumed. The Stern model [21] was the first attempt to incorporate the finite size of ions in EDL theory by combining the Helmholtz [22] and Gouy–Chapman [17,18] models [12,23,24]. Later Bikerman introduced the first complete modified Poisson–Boltzmann (MPB) model which took into consideration the finite size of molecules in the electrolyte solution [25]. This approach was continued by Grimley and Mott [26,27], Freise [28] and Wicke and Eigen [29–31]. Also more recently, the finite size of

the molecules was incorporated into EDL theory using lattice statistics models [3,32,33], by functional density approaches [34–36] and by a modified PB theory where the ions and solvent molecules were treated as hard spheres [14,15,37].

Most of the EDL models published to date are based on the concept that the relative permittivity is constant throughout the whole system [2,12,17,18,38,39]. The dipole moment vectors of water molecules at the charged metal surface are predominantly oriented in an orthogonal direction with respect to the charged surface. This results in a strong local decrease of permittivity [4,5,7,9,14–16,37,40–43], whereas all orientations of water dipoles further away from the charged surface are equally probable.

Considering simultaneously the orientational ordering of water and the finite size of molecules, Outhwaite and co-workers developed a modified PB (MPB) theory of the electrical double layer composed of a mixture of hard spheres with point dipoles and finite sized ions [14,15,37]. Later, Szalai et al. [44] published a mean spherical approximation-based theory [45] that can reproduce simulation results for the electric field dependence of the dielectric permittivity of a dipolar fluid in the saturation regime. The problem was also considered within lattice statistics [16,42,46]. It was shown that due to accumulation of counterions near the charged metal surface, the permittivity in this region is additionally reduced [46].

The Gouy–Chapman (GC) mean-field theory and its Poisson–Boltzmann (PB) equation may be used to estimate the interactions between like-charged surfaces in an electrolyte solution [12,13,47]. For a monovalent salt, it predicts repulsion between like-charged surfaces [58] in agreement with the experimental results and computer simulations. Therefore at first glance, an attractive interaction between two like-charged surfaces would seem impossible. However, the presence of ions with internal charge distribution (mediators) in the intermediate solution between the like-charged surfaces may change the repulsive interaction into an attractive one – not predicted by the mean-field GC approach. The mediators can be charged particles with a quadrupolar internal charge distribution [49–51]. This attraction is currently the subject of much interest because it is observed in a number of biologically relevant processes such as condensation of DNA [52], or the interactions between like-charged lipid membranes that occur during membrane adhesion [53] and fusion [54,55]. Electrostatic attraction between like-charged surfaces is also possible due to direct ion–ion correlations [56,57] in the limit of a high surface charge density and high ion charges [58].

In this review we present a lattice statistics approach to the theory of the EDL. First, we upgrade the description of GC theory and its PB equation by considering the orientational ordering of water molecules near a highly charged surface, the electronic polarizability and the cavity field of water molecules within the Langevin–Poisson–Boltzmann (LPB) model for point-like molecules in electrolyte solution. It is shown that the dielectric permittivity of an electrolyte close to a charged surface is decreased due to the increased orientational ordering of water dipoles. An expression for the osmotic pressure difference between the charged surfaces (Fig. 1) is also derived. The next section is devoted to the effects of ion size of the EDL within the Langevin–Bikerman

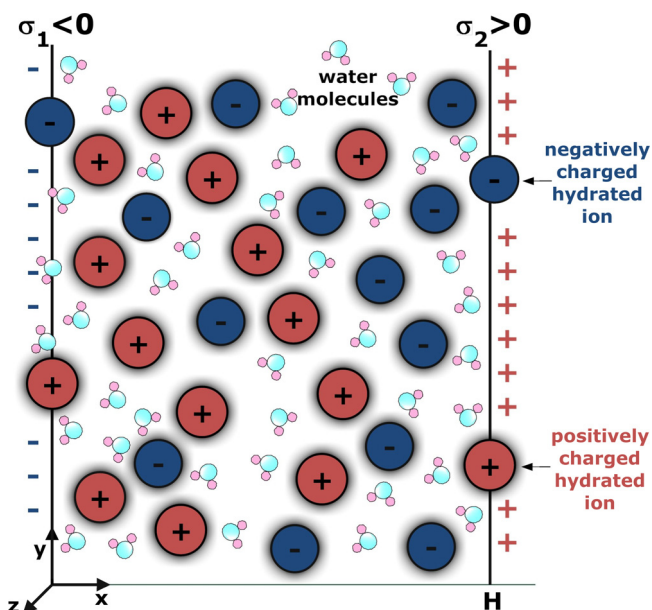


**Fig. 1.** Schematic figure of an electrolyte solution confined between negatively and positively charged surfaces characterized by surface charge densities  $\sigma_1$  at  $x=0$  and  $\sigma_2$  at  $x=H$ . The water dipoles in the vicinity of both charged surfaces are partially oriented towards the surfaces.

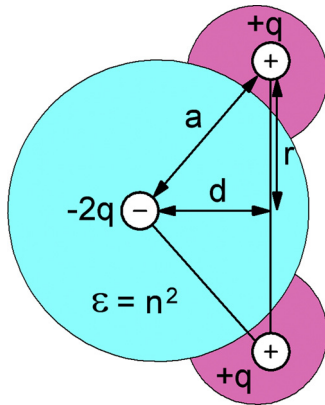


**Fig. 2.** A schematic figure of the charge distribution of a single water molecule within a triangular atomic model. In the model a single water molecule is considered as a sphere with permittivity  $n^2$  and a point-like rigid (permanent) dipole/quadrupole at the centre of the sphere. Here  $n$  is the optical refractive index of water.

Adapted from [59].

(LB) model. It is shown that the dielectric permittivity close to the charged surface is additionally decreased due to the finite size of ions and dipoles in the electrolyte solution. We also shed light on the effect of finite-sized ions and water molecules on the osmotic pressure between charged surfaces in contact with the intermediate electrolyte solution. In the last part of this section we show that unlike the unphysical prediction of the GC model, the calculated differential capacitance within the MLB model, after reaching its maximum, decreases with increasing surface potential in accordance with experimental observations. In the next section the LPB model is generalized to describe the zwitterionic lipid layer in contact with an electrolyte solution where some of the model predictions are critically evaluated using the molecular dynamics (MD) simulation. The end of this section is dedicated to study of the interaction of positively and negatively charged macroions with the zwitterionic lipid layer. At the end of the article, we discuss the possible origins of attractive interactions between two like-charged surfaces immersed in a solution of macroions with spatially distributed internal charge. The final section rounds off the work by drawing final inferences, and pointing to future work and possible applications of the models described.

## 2. Energy of a single water molecule within a triangular atomic model

In the triangular atomic model of water, electronic polarization is taken into account by assuming that the point-like and rigid (permanent) dipole/quadrupole is embedded in the centre of a sphere with a volume equal to the average volume of a water molecule in an electrolyte solution, as shown schematically in Fig. 2. The permittivity of the sphere is taken to be  $n^2$ , where  $n = 1.33$  is the optical refractive index of water [46,59,60]. The energy of a single water molecule can be written as (see Fig. 3):

$$W(x) = -2q\phi_c \left( x - \frac{d}{2} \cos \omega \right) + q\phi_c \left( x - \frac{d}{2} \cos \omega + a \cos(\omega + \varphi) \right) + q\phi_c \left( x - \frac{d}{2} \cos \omega + a \cos(\omega - \varphi) \right), \quad (1)$$

where  $+q$  and  $-q$  are point charges,  $\phi_c$  is the local (cavity) electric potential,  $d$  and  $a$  are the distances and  $\omega$  and  $\varphi$  the angles as denoted in Figs. 2 and 3.

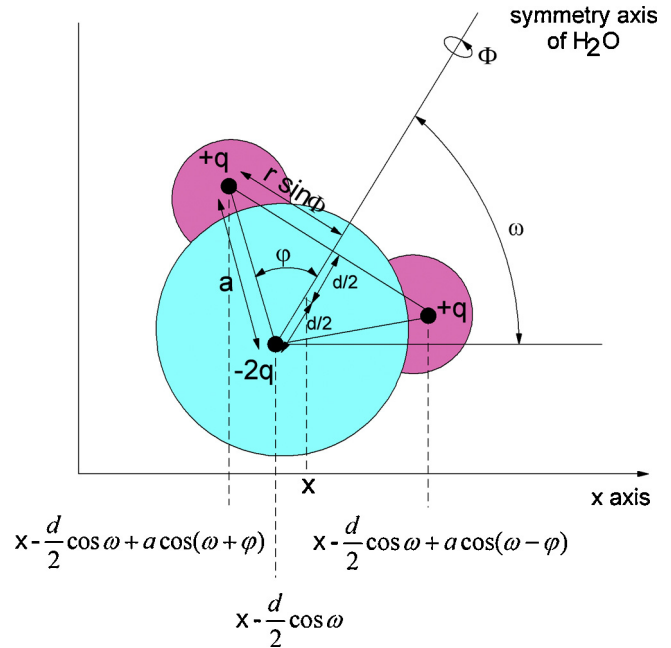


**Fig. 3.** Geometrical parameters of the triangular atomic model of a water molecule. Adapted from [59].

For small  $d$  and  $a$ , we can expand the energy  $W(x)$  in Eq. (1) into a Taylor series up to the quadratic terms [59]:

$$W(x) = p \cos \omega |\phi'_c(x)| + qr^2 \sin^2 \Phi \sin^2 \omega |\phi''_c(x)|, \quad (2)$$

where  $d = a \cos \varphi$ ,  $a \sin \varphi = r \sin \Phi$ ,  $p = 2qd$  is the magnitude of the internal dipole,  $qr^2$  characterizes the internal quadrupole, while  $\omega$  is the angle between the gradient of the electric potential  $\phi'_c(x)$  and the vector of the water dipole moment.

Fig. 4 shows the dependence of the average cosine  $\langle \cos(\omega) \rangle_B$  (Eq. (11)) and the magnitude of the electric field strength  $E(x)$  as a function of the distance from the charged surface at  $x=0$ . The spatial dependence of  $E(x)$  is determined within the Langevin–Bikerman model from the spatial dependence of the electric potential calculated from the Gongadze–Iglič (GI) equation (Eq. (43)), as described later in Section 4 of this review. It can be seen that the magnitude of  $\langle \cos(\omega) \rangle_B$  increases with decreasing distance from the charged surface and increasing magnitude of the surface charge density  $\sigma$ . This is because the magnitude of the electric field  $E(x)$  is strongly increased in the vicinity of the charged surface (Fig. 4). The tendency to increasing  $E(x)$  in the direction towards the charged surface is more pronounced for larger magnitudes of  $\sigma$ .

## 3. Point-like molecules in an electrolyte solution

### 3.1. Modified Langevin–Poisson–Boltzmann equation

In this section we describe the modified Langevin–Poisson–Boltzmann (MLPB) model of the EDL [42,61] considering molecules of the electrolyte solution as point-like particles. For reasons of simplicity we neglect the internal quadrupole energy term (i.e. the second term in Eq. (2)) so that the energy of a single water molecule in the local field  $W(\omega)$  is given by:

$$W(\omega) = pE_c \cos \omega, \quad (3)$$

where  $E_c$  is the magnitude of the local cavity electric field  $\phi'_c(x)$ . If the short range interactions between water molecules are neglected, the local electric field strength at the centre of the single

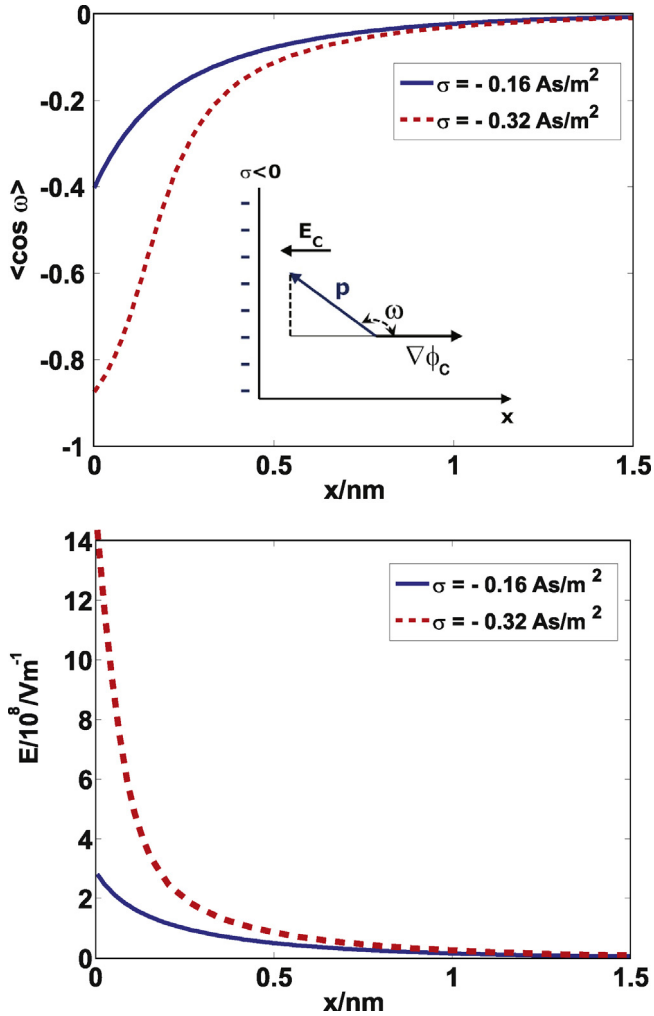


**Fig. 4.** Average orientation of water molecules described by  $\langle \cos(\omega) \rangle_B$  (upper panel) and the magnitude of the electric field strength  $E(x)$  (lower panel) as a function of the distance from the charged plate ( $x$ ) calculated within the LB model using the GI for two values of the surface charge density  $\sigma$ :  $e_0/nm^2 = -0.16 \text{ As/m}^2$  (full lines) and  $2e_0/nm^2 = -0.32 \text{ As/m}^2$  (dashed lines). Values of parameters: bulk concentration of salt  $n_0/N_A = 0.5 \text{ mol/l}$ , dipole moment of water  $p_0 = 3.1 \text{ D}$ , optical refractive index  $n = 1.33$ , bulk concentration of water  $n_{ow}/N_A = 55 \text{ mol/l}$ .

water molecule sphere (cavity) with dielectric permittivity  $n^2$  at the location of the permanent (rigid) point-like dipole is [60]:

$$E_c = \frac{3\varepsilon_r}{2\varepsilon_r + n^2} E, \quad (4)$$

where  $E$  is the magnitude of the external field. The water molecules are embedded in a medium with permittivity  $\varepsilon_r$ . Eq. (4) is further simplified to the form (strictly valid for  $\varepsilon_r \gg n^2$  only):  $E_c = (3/2)E$ . The energy of the point-like dipole  $p$  in the local cavity field of magnitude  $E_c$  may then be rewritten as:

$$W_i = \gamma p_0 E \cos(\omega), \quad (5)$$

where  $p_0$  is the magnitude of the external dipole moment  $p_e = (3/(2+n^2))p$  [46,60] and  $\gamma$  is given by [46]:

$$\gamma = \frac{3}{2} \left( \frac{2+n^2}{3} \right). \quad (6)$$

In the LPB and MLPB models described in this section, the dielectric permittivity is consistently related to the orientational ordering of water molecules, while the finite volume of ions and water, i.e. the excluded volume effect, is not taken into account. The volume

density of water ( $n_w(x)$ ) is therefore constant over the whole electrolyte solution [3,42], while the number densities of counterions ( $n_+(x)$ ) and coions ( $n_-(x)$ ) are described by the Boltzmann distribution functions [3,17,18]:

$$n_+(x) = n_0 e^{-e_0\phi\beta}, \quad (7)$$

$$n_-(x) = n_0 e^{e_0\phi\beta}, \quad (8)$$

$$n_w(x) = n_{0w}, \quad (9)$$

where  $n_{0w}$  is the constant (bulk) number density of water and  $n_0$  the bulk number density of counterions and coions of electrolyte solution, and  $\beta = 1/kT$ , where  $kT$  is the thermal energy. The polarization in the vicinity of a negatively charged surface (see Fig. 1) is then given by [42]:

$$\begin{aligned} P(x) &= n_{0w} \left( \frac{2+n^2}{3} \right) p_0 \langle \cos(\omega) \rangle_B \\ &= -n_{0w} \left( \frac{2+n^2}{3} \right) p_0 \mathcal{L}(\gamma p_0 E \beta), \end{aligned} \quad (10)$$

where  $\mathcal{L}(u)$  is Langevin function and  $\langle \cos(\omega) \rangle_B$  is (see [60]):

$$\langle \cos(\omega) \rangle_B = \frac{\int_0^\pi \cos \omega \mathcal{P}(x, \omega) 2\pi \sin \omega d\omega}{\int_0^\pi \mathcal{P}(x, \omega) 2\pi \sin \omega d\omega} = -\mathcal{L}(\gamma p_0 E \beta). \quad (11)$$

Combining the definition of the relative (effective) permittivity  $\varepsilon_r(x) = n^2 + |P|/\varepsilon_0 E$  and Eq. (10) gives [42,61]:

$$\varepsilon_r(x) = n^2 + \frac{|P|}{\varepsilon_0 E} = n^2 + \frac{n_{0w} p_0}{\varepsilon_0} \left( \frac{2+n^2}{3} \right) \frac{\mathcal{L}(\gamma p_0 E(x) \beta)}{E(x)}, \quad (12)$$

Using Eq. (12) for the space-dependent relative permittivity  $\varepsilon_r(x)$ , we can rewrite the MLPB equation in the form [42,61]:

$$\frac{d}{dx} \left[ \varepsilon_0 \varepsilon_r(x) \frac{d\phi}{dx} \right] = 2e_0 n_0 \sinh(e_0\phi\beta), \quad (13)$$

where the macroscopic (net) volume charge density of coions and counterions in the form:

$$\rho_{free}(x) = -e_0 n_+(x) - e_0 n_-(x) = -2e_0 n_0 \sinh(e_0\phi\beta), \quad (14)$$

was taken into account. The boundary conditions are [42,61] (see also Fig. 1):

$$\frac{d\phi}{dx} (x=0) = -\frac{\sigma_1}{\varepsilon_0 \varepsilon_r(x=0)}, \quad (15)$$

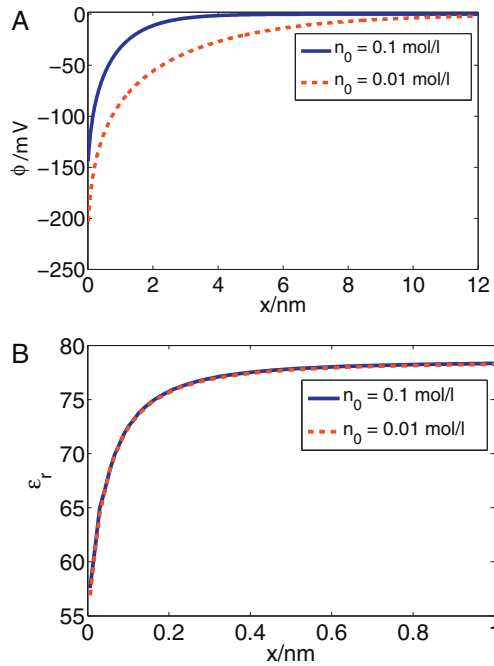
$$\frac{d\phi}{dx} (x=H) = +\frac{\sigma_2}{\varepsilon_0 \varepsilon_r(x=H)}. \quad (16)$$

Fig. 5 shows the spatial dependence of the electric potential  $\phi(x)$  and relative permittivity  $\varepsilon_r$  in planar geometry for two values of the bulk number density of counterions and coions  $n_0$ . A considerable decrease of relative permittivity can be observed in the close vicinity of the charged surface.

In the limit of a vanishing electric field strength ( $E(x) \rightarrow 0$ ) everywhere in the solution, Eq. (12) for the relative permittivity  $\varepsilon_{r,b}(x)$  gives the classical Onsager expression [62]:

$$\varepsilon_{r,b} \cong n^2 + \left( \frac{2+n^2}{3} \right)^2 \frac{n_{0w} p_0^2 \beta}{2\varepsilon_0}. \quad (17)$$

At room temperature (298 K),  $p_0 = 3.1 \text{ Debye}$  (the Debye is  $3.336 \times 10^{-30} \text{ C/m}$ ) and  $n_{0w}/N_A = 55 \text{ mol/l}$ , Eq. (17) gives  $\varepsilon_{r,b} = 78.5$  for bulk solution. The value  $p_0 = 3.1 \text{ Debye}$  is considerably smaller than the corresponding value in previous similar models ( $p_0 = 4.79 \text{ D}$ ) [42,63,64] which did not take into account the cavity field and electronic polarizability of water molecules.



**Fig. 5.** Electric potential  $\phi(x)$  (upper panel) and relative permittivity  $\varepsilon_r(x)$  (lower panel) as a function of the distance from a negatively charged surface  $x=0$  (see Fig. 1) and large  $H$  calculated within the MLPB model for two values of the bulk concentration of counterions and coions  $n_0/N_A$ : 0.1 mol/l and 0.01 mol/l. The model parameters are:  $\sigma_1 = -0.3 \text{ As/m}^2$ ,  $T = 298 \text{ K}$ ,  $p_0 = 3.1$  Debye, concentration of water  $n_{0w}/N_A = 55 \text{ mol/l}$ , where  $N_A$  is the Avogadro number. The MLPB Eq. (13) was solved numerically as described in [42,46].

### 3.2. Langevin–Poisson–Boltzmann equation

Neglecting the influence of the cavity field, the MLPB equation (Eq. (13)) [61] transforms into LPB equations [42] valid in the limit of  $\gamma \rightarrow 1$  and  $n \rightarrow 1$  to obtain [16,42]:

$$\frac{d}{dx} \left[ \varepsilon_0 \varepsilon_r(x) \frac{d\phi}{dx} \right] = 2e_0 n_0 \sinh(e_0 \phi \beta), \quad (18)$$

where the space dependent relative permittivity  $\varepsilon_r(x)$  is [16,42]:

$$\varepsilon_r(x) = 1 + \frac{n_{0w} p_0}{\varepsilon_0} \frac{\mathcal{L}(p_0 E \beta)}{E}. \quad (19)$$

Eq. (18) differs from Eq. (13) in the expression for  $\varepsilon_r(x)$  which is not the same in the two cases. In the limit of vanishing electric field strength ( $E \rightarrow 0$ ), Eq. (19) predicts:

$$\varepsilon_{r,b} \cong 1 + \frac{n_{0w} p_0^2 \beta}{3 \varepsilon_0}. \quad (20)$$

At room temperature (298 K),  $p_0 = 4.79 \text{ D}$  and  $n_{0w}/N_A = 55 \text{ mol/l}$  Eq. (20) gives  $\varepsilon_{r,b} = 78.5$  for bulk solution. The value of the dipole moment  $p_0 = 4.79 \text{ D}$  [42,63,64] is considerably larger than the corresponding value in the above described MLPB model ( $p_0 = 3.1 \text{ D}$ ) which takes into account the cavity field and electronic polarizability of water molecules [46,61].

### 3.3. Limiting Poisson–Boltzmann equation

Assuming a constant bulk value of the permittivity everywhere in the electrolyte solution, including the close vicinity of charged surfaces, the LPB equation transforms into the PB equation [17,18]:

$$\varepsilon_0 \varepsilon_r \frac{d^2 \phi}{dx^2} = 2e_0 n_0 \sinh(e_0 \phi \beta). \quad (21)$$

### 3.4. Osmotic pressure

In the following we derive an expression for the osmotic pressure difference between the charged surfaces as presented in Fig. 1. To this end Eq. (13) of the MLPB is first integrated (see also [47]) and then in the second step the corresponding bulk value of the pressure is subtracted from the local pressure to get the osmotic pressure  $\Pi$ . Prior to its integration, Eq. (13) is rearranged in the form (see also [42]):

$$\begin{aligned} & -\frac{d}{dx} \left[ \varepsilon_0 n^2 \frac{d\phi}{dx} \right] + 2e_0 n_0 \sinh e_0 \phi \beta \\ & - n_{0w} p_0 \left( \frac{2+n^2}{3} \right) \frac{d}{dx} (\mathcal{L}(\gamma p_0 E \beta)) = 0. \end{aligned} \quad (22)$$

Eq. (22) is multiplied by  $\phi' \equiv d\phi/dx$  and integrated [47] to get the first integral equivalent to the contact theorem:

$$\begin{aligned} & \frac{1}{2} \varepsilon_0 n^2 E(x)^2 + 2n_0 kT (\cosh(-e_0 \phi(x) \beta)) \\ & - E(x) \left( \frac{2+n^2}{3} \right) n_{0w} p_0 \mathcal{L}(\gamma p_0 E(x) \beta) \\ & + \left( \frac{2+n^2}{3} \right) \frac{n_{0w}}{\gamma \beta} \ln \left( \frac{\sinh(\gamma p_0 E(x) \beta)}{\gamma p_0 E(x) \beta} \right) = const, \end{aligned} \quad (23)$$

where  $const$  is the local pressure between the charged surfaces (as defined in Fig. 1). In the derivation of Eq. (23) the relations

$$\int \phi'' \phi' dx = \int \frac{1}{2} d(\phi')^2 = \frac{1}{2} (\phi')^2, \quad \int \frac{d\mathcal{L}}{dx} \phi' dx = \mathcal{L} \phi' - \int \mathcal{L} d\phi',$$

are used. Here  $\phi'' \equiv d^2 \phi/dx^2$  and  $d\phi = \phi' dx$ . By subtracting the corresponding bulk values from the local pressure we obtain the expression for the osmotic pressure difference within the MLPB model [65]:

$$\begin{aligned} \Pi_{MLPB} = & -\frac{1}{2} \varepsilon_0 n^2 E(x)^2 + 2n_0 kT (\cosh(-e_0 \phi(x) \beta) - 1) \\ & - E(x) \left( \frac{2+n^2}{3} \right) n_{0w} p_0 \mathcal{L}(\gamma p_0 E(x) \beta) \\ & + \left( \frac{2+n^2}{3} \right) \frac{n_{0w}}{\gamma \beta} \ln \left( \frac{\sinh(\gamma p_0 E(x) \beta)}{\gamma p_0 E(x) \beta} \right). \end{aligned} \quad (24)$$

Substituting the spatial number density distributions for cations and anions of the electrolyte solution:

$$n_+(x) = n_0 \exp(-e_0 \phi(x) \beta), \quad n_-(x) = n_0 \exp(e_0 \phi(x) \beta), \quad (25)$$

Eq. (24) reads:

$$\begin{aligned} \Pi_{MLPB} = & -\frac{1}{2} \varepsilon_0 n^2 E(x)^2 + kT(n_+(x) + n_-(x) - 2n_0) \\ & - E(x) \left( \frac{2+n^2}{3} \right) n_{0w} p_0 \mathcal{L}(\gamma p_0 E(x) \beta) \\ & + \left( \frac{2+n^2}{3} \right) \frac{n_{0w}}{\gamma \beta} \ln \left( \frac{\sinh(\gamma p_0 E(x) \beta)}{\gamma p_0 E(x) \beta} \right). \end{aligned} \quad (26)$$

For small  $\gamma p_0 E(x) \beta$  we can expand the 3rd and 4th terms in Eq. (26) into Taylor series to get:

$$\begin{aligned} \Pi_{MLPB} \approx & -\frac{1}{2} \varepsilon_0 \left( n^2 + \left( \frac{2+n^2}{3} \right)^2 \frac{n_{0w} p_0^2 \beta}{2 \varepsilon_0} \right) E(x)^2 \\ & + kT(n_+(x) + n_-(x) - 2n_0). \end{aligned} \quad (27)$$

Using the Onsager expression for bulk relative permittivity (Eq. (17)), Eq. (27) can be rewritten in the usual PB form for the osmotic

pressure within the EDL theory [58]:

$$\begin{aligned} \Pi_{PB} &= -\frac{1}{2} \varepsilon_0 \varepsilon_{r,b} E(x)^2 + kT(n_+(x) + n_-(x) - 2n_0) \\ &= -\frac{1}{2} \varepsilon_0 \varepsilon_{r,b} E(x)^2 + 2n_0 kT(\cosh(e_0 \phi(x)\beta) - 1). \end{aligned} \quad (28)$$

Following a procedure similar to that in the case of derivation of Eq. (24), one can also derive the corresponding expression for osmotic pressure by integrating Eq. (18) of the LPB (see also [47]) to get:

$$\begin{aligned} \Pi_{LPB} &= -\frac{1}{2} \varepsilon_0 n^2 E(x)^2 + kT(n_+(x) + n_-(x) - 2n_0) \\ &\quad - E(x)n_{0w} p_0 \mathcal{L}(p_0 E(x)\beta) + \frac{n_{0w}}{\beta} \ln \left( \frac{\sinh(p_0 E(x)\beta)}{p_0 E(x)\beta} \right). \end{aligned} \quad (29)$$

One can also derive Eq. (29) directly from Eq. (24) in the limit of  $\gamma \rightarrow 1$  and  $n \rightarrow 1$ . For small  $p_0 E(x)\beta$  we can expand the 3rd and 4th terms in Eq. (29) into Taylor series to get:

$$\Pi_{LPB} \approx -\frac{1}{2} \varepsilon_0 \left( 1 + \frac{n_{0w} p_0^2 \beta}{3 \varepsilon_0} \right) E(x)^2 + kT(n_+(x) + n_-(x) - 2n_0). \quad (30)$$

Taking into account Eq. (20), the above Eq. (30) attains the PB form of the equation for osmotic pressure, i.e. the form of Eq. (28).

The osmotic pressure is constant everywhere in the solution between the charged plates. In the case of like charged surfaces where  $\sigma_1$  at  $x=0$  and  $\sigma_2$  at  $x=H$  (Fig. 1) are both negative or positive and equal ( $\sigma_1 = \sigma_2$ ), the electric field strength at  $x=H/2$  is zero, therefore the expression for osmotic pressure within the PB (Eq. (28)), LPB (Eq. (29)) and MLPB model (Eq. (26)) simplifies to:

$$\begin{aligned} \Pi_i(x=H/2) &= \frac{2n_0}{\beta} (\cosh(e_0 \phi_i(x=H/2)\beta) - 1), \\ i &= PB, LPB, MLPB. \end{aligned} \quad (31)$$

where  $\phi_{PB}(x=H/2)$ ,  $\phi_{LPB}(x=H/2)$  and  $\phi_{MLPB}(x=H/2)$  are calculated from the PB, LPB and MLPB equations, respectively.

Fig. 6 shows the osmotic pressure between negatively and positively charged surfaces (upper panel) and between two negatively charged surfaces (lower panel) (see also Fig. 1) as a function of the decreasing distance ( $H$ ) between them, calculated within the MLPB model (Eq. (24)). The decrease of the osmotic pressure  $\Pi(H)$  is more pronounced for smaller values of the bulk concentration of salt. The predicted values of the osmotic pressure within the MLPB model differ from the corresponding values within the standard PB model only at very small distances  $H$ , where within the MLPB model the influence of the space variation of permittivity at both charged surfaces (see Eq. (12)) on the osmotic pressure is not negligible.

#### 4. Finite-sized molecules in an electrolyte solution

Unlike in the LPB model, in this section the finite volume of the molecules is taken into account.

##### 4.1. Gongadze–Iglič equation

Since in bulk solution the number densities of water molecules ( $n_{0w}$ ), counterions ( $n_0$ ) and co-ions ( $n_0$ ) are constant, their number densities can be expressed in a simple way by calculating the corresponding probabilities that a single lattice site in the bulk solution is occupied by one of the three kinds of particles in the electrolyte solution (counterions, co-ions and water molecules) [16,20,24]. However, in the vicinity of a charged surface the number densities of ions and water molecules are influenced by the charged surface

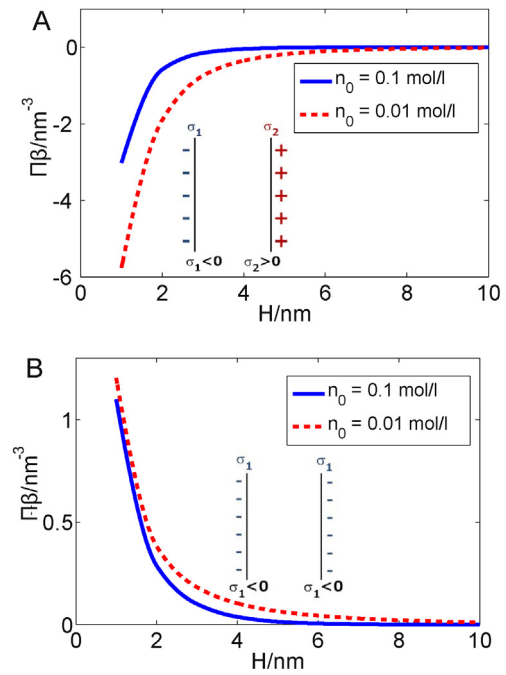


**Fig. 6.** Osmotic pressure between negatively and positively charged surfaces (upper panel) and between two negatively charged surfaces (lower panel) as a function of the distance between the two surfaces ( $H$ ) (see Fig. 1), calculated within the MLPB model (Eq. (24)) for two values of the bulk salt concentration  $n_0/N_A = 0.01$  mol/l (dashed lines) and  $n_0/N_A = 0.1$  mol/l (full lines). Other model parameters are:  $\sigma_1 = -0.2$  As/m<sup>2</sup>,  $\sigma_2 = 0.2$  As/m<sup>2</sup>,  $T = 298$  K, concentration of water  $n_{0w}/N_A = 55$  mol/l and dipole moment of water  $p_0 = 3.1$  Debye, where  $N_A$  is the Avogadro number.

(see also Fig. 1), so the probabilities that a single lattice site is occupied by a particle of one of the three kinds should be corrected by the corresponding Boltzmann factors, leading to ion and water dipole distribution functions in the form [46]:

$$n_+(x) = n_s \frac{n_0 e^{-e_0 \phi \beta}}{n_0 e^{e_0 \phi \beta} + n_0 e^{-e_0 \phi \beta} + n_{0w} \langle e^{-\gamma p_0 E \beta \cos(\omega)} \rangle_\omega}, \quad (32)$$

$$n_-(x) = n_s \frac{n_0 e^{e_0 \phi \beta}}{n_0 e^{e_0 \phi \beta} + n_0 e^{-e_0 \phi \beta} + n_{0w} \langle e^{-\gamma p_0 E \beta \cos(\omega)} \rangle_\omega}, \quad (33)$$

$$n_w(x) = n_s \frac{n_{0w} \langle e^{-\gamma p_0 E \beta \cos(\omega)} \rangle_\omega}{n_0 e^{e_0 \phi \beta} + n_0 e^{-e_0 \phi \beta} + n_{0w} \langle e^{-\gamma p_0 E \beta \cos(\omega)} \rangle_\omega}, \quad (34)$$

where  $n_s$  is the number density of lattice sites defined as  $2n_0 + n_{0w}$  and

$$\langle e^{-\gamma p_0 E \beta \cos(\omega)} \rangle_\omega = \frac{2\pi \int_{-\pi}^0 d(\cos \omega) e^{-\gamma p_0 E \beta \cos(\omega)}}{4\pi} = \frac{\sinh(\gamma p_0 E \beta)}{\gamma p_0 E \beta}, \quad (35)$$

is the dipole Boltzmann factor after rotational averaging over all possible angles  $\omega$ . Eqs. (32)–(34) can be rewritten as [46]:

$$n_+(x) = n_0 e^{-e_0 \phi \beta} \frac{n_s}{\mathcal{D}(\phi, E)}, \quad (36)$$

$$n_-(x) = n_0 e^{e_0 \phi \beta} \frac{n_s}{\mathcal{D}(\phi, E)}, \quad (37)$$

$$n_w(x) = \frac{n_{0w} n_s}{\mathcal{D}(\phi, E)} \frac{\sinh(\gamma p_0 E \beta)}{\gamma p_0 E \beta}. \quad (38)$$

where  $\mathcal{D}(\phi, E) = 2n_0 \cosh(e_0\phi\beta) + (n_{0w}/\gamma p_0 E\beta) \sinh(\gamma p_0 E\beta)$ . Combining Eq. (10)

$$P(x) = -n_w(x) \left( \frac{2+n^2}{3} \right) p_0 \mathcal{L}(\gamma p_0 E\beta), \quad (39)$$

and Eq. (38) gives the polarization in the form:

$$P(x) = - \left( \frac{2+n^2}{3} \right) \frac{p_0 n_{0w} n_s}{\mathcal{D}(\phi, E)} \frac{\mathcal{L}(\gamma p_0 E\beta)}{\gamma p_0 E\beta} \sinh(\gamma p_0 E\beta). \quad (40)$$

Using the definition of the function  $\mathcal{F}(u)$ :  $\mathcal{F}(u) = \mathcal{L}(u)(\sinh u/u)$ , Eq. (40) transforms into:

$$P = -p_0 n_{0w} n_s \left( \frac{2+n^2}{3} \right) \frac{\mathcal{F}(\gamma p_0 E\beta)}{\mathcal{D}(\phi, E)}. \quad (41)$$

Combining  $\varepsilon_r(x) = n^2 + |P|/\varepsilon_0 E$  and Eq. (41) yields the relative (effective) permittivity [46]:

$$\varepsilon_r(x) = n^2 + n_{0w} n_s \frac{p_0}{\varepsilon_0} \left( \frac{2+n^2}{3} \right) \frac{\mathcal{F}(\gamma p_0 E\beta)}{\mathcal{D}(\phi, E) E}. \quad (42)$$

Using the above expression for  $\varepsilon_r(x)$ , we can then write the Poisson equation into the Gongadze-Iglić (GI) equation in the form [16,46]:

$$\frac{d}{dx} \left[ \varepsilon_0 \varepsilon_r(x) \frac{d\phi}{dx} \right] = 2 e_0 n_s n_0 \frac{\sinh(e_0\phi\beta)}{\mathcal{D}(\phi, E)}, \quad (43)$$

where the macroscopic (net) volume charge density of co-ions and counterions  $\rho_{free}(x)$  (Eqs. (36) and (37)) [46] was taken into account:

$$\rho_{free}(x) = e_0 n_+(x) - e_0 n_-(x) = -2 e_0 n_s n_0 \frac{\sinh(e_0\phi\beta)}{\mathcal{D}(\phi, E)}. \quad (44)$$

The boundary conditions are (see also Fig. 1):

$$\frac{d\phi}{dx}(x=0) = -\frac{\sigma_1}{\varepsilon_0 \varepsilon_r(x=0)}, \quad (45)$$

$$\frac{d\phi}{dx}(x=H) = +\frac{\sigma_2}{\varepsilon_0 \varepsilon_r(x=H)}, \quad (46)$$

where  $\varepsilon_r(x)$  is defined by Eq. (42).

In the limit of vanishing electric field strength ( $E \rightarrow 0$ ) and zero potential ( $\phi \rightarrow 0$ ), the above derived expression for relative permittivity (Eq. (42)) gives the well-known Onsager expression for permittivity [62]:

$$\varepsilon_{r,b} \cong n^2 + \left( \frac{2+n^2}{3} \right)^2 \frac{n_{0w} p_0^2 \beta}{2 \varepsilon_0}. \quad (47)$$

It is worth noting that using Eq. (42) the value of the dipole moment  $p_0 = 3.1$  D predicts a bulk permittivity of  $\varepsilon_r = 78.5$ .

In Fig. 7 we show the number density of counter ions  $n_+(x)$  and water dipoles  $n_w(x)$  as a function of the distance from a negatively planar charged surface  $x$ . The predicted depletion of water molecules near the charged surface is due to accumulation of counterions close to the charged surface in accordance with the excluded volume principle taken into account in the Langevin–Bikerman model.

In Fig. 8 we demonstrate the spatial dependences of the electric potential  $\phi(x)$  and relative permittivity  $\varepsilon_r(x)$ . The decrease of relative permittivity  $\varepsilon_r(x)$  towards the charged surface is a consequence of the increased orientational ordering of water dipoles (saturation effect) close to the charged surface (Fig. 4) and the increased depletion of water molecules near the charged surface due to accumulation of counterions (see Fig. 7). The decrease of  $\varepsilon_r(x)$  near the charged surface is more pronounced for larger magnitudes of the surface charge density ( $\sigma$ ) (Fig. 9) due to stronger water ordering at larger  $|\sigma|$ , as presented in Fig. 4.

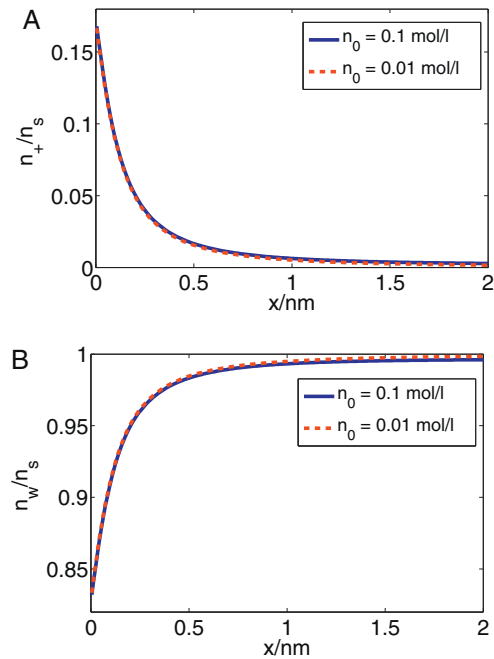


**Fig. 7.** The relative number density of counterions ( $n_+/n_s$ ) (upper panel) and water dipoles ( $n_w/n_s$ ) (lower panel) (calculated using Eqs. (36) and (38)) as a function of the distance from a planar charged surface  $x$  calculated for two values of the bulk concentration of counterions and coions  $n_0/N_A$ : 0.1 mol/l (full lines) and 0.01 mol/l (dashed lines). Values of parameters assumed:  $\sigma = -0.2$  As/m<sup>2</sup>, dipole moment of water  $p_0 = 3.1$  D, optical refractive index  $n = 1.33$ , bulk concentration of water  $n_{0w}/N_A = 55$  mol/l, where  $N_A$  is the Avogadro number. The GI equation (43) was solved numerically as described in [46].

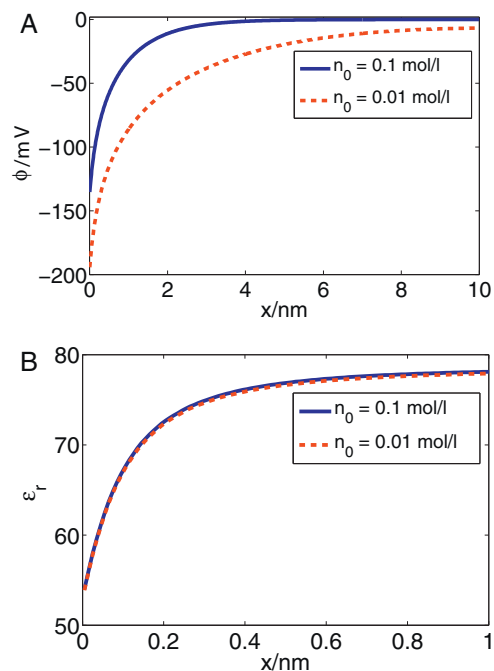


**Fig. 8.** Electric potential  $\phi(x)$  (upper panel) and relative permittivity  $\varepsilon_r(x)$  (lower panel) as a function of the distance from the negatively charged surfaces at  $x=0$  (see Fig. 1) and at large  $H$  calculated for two values of the bulk concentration of counterions and coions  $n_0/N_A$ : 0.1 mol/l (full lines) and 0.01 mol/l (dashed lines). The values of model parameters are the same as given in Fig. 7. The GI equation (43) was solved numerically as described in [46].

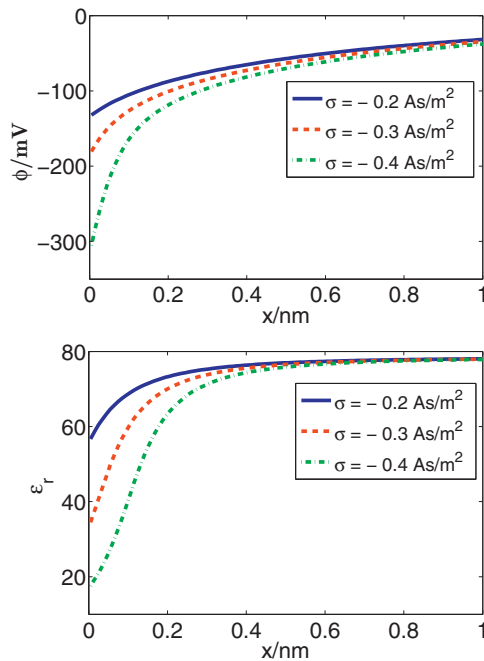


**Fig. 9.** Electric potential  $\phi(x)$  (upper panel) and relative permittivity  $\varepsilon_r(x)$  (lower panel) as a function of the distance from the negatively charged surfaces at  $x=0$  (see Fig. 1) and at large  $H$  calculated for three values of the surface charge density  $\sigma = -0.2 \text{ As/m}^2$  (full lines),  $\sigma = -0.3 \text{ As/m}^2$  (dashed lines) and  $\sigma = -0.4 \text{ As/m}^2$  (dash-dotted lines) at the bulk concentration of counterions and coions  $n_0/N_A = 0.15 \text{ mol/l}$  and  $p_0 = 4.79 \text{ D}$ . The values of other model parameters are the same as given at Fig. 7. The LB equation (48) was solved numerically as described in [46].

Comparing the decrease of relative permittivity at the charged surface  $\varepsilon_r(x \approx 0)$  shows that at same (and large enough)  $\sigma$  in the MLB model (Fig. 9)  $\varepsilon_r(x \approx 0)$  attains a much lower value than in the MLPB model Fig. 5. The observed difference in the predictions of the MLB and MLPB models is the consequence of the depletion of the number density of water molecules in the vicinity of the negatively charged surface ( $n_+(x \approx 0)$ ) (see Fig. 7), which is then reflected in a substantial decrease of the magnitude of polarization (see Eq. (39)) and therefore also in a decrease of  $\varepsilon_r(x \approx 0)$ .

To estimate experimentally the spatial dependence of the dielectric permittivity ( $\varepsilon_r(x)$ ), an appropriate theoretical model and model parameters should be adopted [66,67]. This means that the experimentally obtained value of  $\varepsilon_r(x)$  depends substantially on the type of theoretical model selected. To this end it is debatable whether the thickness of the oriented water layer near the charged surface is around or below 1 nanometre or a few tens of nanometres (see for example [67] and references therein). Teschke et al. [67] used atomic force microscopy and an appropriate theoretical analysis in order to determine the permittivity of an electrolyte solution at a negatively charged mica surface, i.e. at  $x=0$ . The value  $\varepsilon_r(x=0) \leq 10$  was obtained for different kinds of electrolyte solutions in contact with the mica surface [67]. The measured permittivity  $\varepsilon_r(x)$  increased with distance from the mica surface to reach a bulk value of  $\sim 80$  at about 10 nm from the mica surface [66,67]. The estimated value  $\varepsilon_r(x=0) \sim 10$  [67] is larger than the corresponding values predicted within the LPB and LB models calculated for  $\sigma \simeq -0.1$  to  $-0.2 \text{ As/m}^2$  as assumed by Teschke et al. [67]. Also the theoretically predicted (by the GI model) thickness of the region of oriented water molecules (coinciding with the region of spatial variation of  $\varepsilon_r$ ) is considerably thinner than the experimental value determined by Teschke et al. [67]. A value of  $\varepsilon_r(x=0)$  around 10 can be predicted by the GI equation, but only for  $|\sigma| > 0.2 \text{ As/m}^2$ . It is possible that the  $|\sigma|$  value adopted in

[67] is too small, since it may be influenced by different factors such as, for example, adhesion of ions to the charged surface [5]. However, it is also possible that the simplifications adopted in the theoretical models discussed, such as for example neglecting direct interactions between water dipoles, are the partial origin of these discrepancies. Interestingly, the smaller value of  $\varepsilon_r(x=0)$  (around 10) can be predicted within the theoretical approach presented by taking into account the quadrupole moment of water molecules [59] (see also Fig. 2).

#### 4.2. Langevin–Bikerman equation

The above described GI equation (Eq. (43)) [46] may be written in the limit of  $\gamma \rightarrow 1$  and  $n \rightarrow 1$  [16,42] to obtain the Langevin–Bikerman equation [42,64]:

$$\frac{d}{dx} \left[ \varepsilon_0 \varepsilon_r(x) \frac{d\phi}{dx} \right] = 2 e_0 n_s n_0 \frac{\sinh(e_0 \phi \beta)}{\mathcal{H}(\phi, E)}, \quad (48)$$

where the macroscopic (net) volume charge density of co-ions and counterions  $\rho_{free}(x)$  in the form:

$$\rho_{free}(x) = -2 e_0 n_s n_0 \frac{\sinh(e_0 \phi \beta)}{\mathcal{H}(\phi, E)}, \quad (49)$$

is taken into account, while the relative permittivity  $\varepsilon_r(x)$  is [16,63,64]:

$$\varepsilon_r(x) = 1 + n_{0w} n_s \frac{p_0 \mathcal{F}(p_0 E \beta)}{\varepsilon_0 E \mathcal{H}(\phi, E)}, \quad (50)$$

where

$$\mathcal{H}(\phi, E) = 2 n_0 \cosh(e_0 \phi \beta) + \frac{n_{0w}}{p_0 E \beta} \sinh(p_0 E \beta). \quad (51)$$

The corresponding number densities of counterions, coions and water molecules are [16,64]:

$$n_+(x) = n_0 e^{-e_0 \phi \beta} \frac{n_s}{\mathcal{H}(\phi, E)}, \quad (52)$$

$$n_-(x) = n_0 e^{e_0 \phi \beta} \frac{n_s}{\mathcal{H}(\phi, E)}, \quad (53)$$

$$n_w(x) = \frac{n_{0w} n_s}{\mathcal{H}(\phi, E)} \frac{1}{p_0 E \beta} \sinh(p_0 E \beta). \quad (54)$$

In the limit of vanishing electric field strength ( $E \rightarrow 0$ ) and vanishing electric potential ( $\phi \rightarrow 0$ ) Eq. (50) transforms into:

$$\varepsilon_{r,b} \simeq 1 + \frac{n_{0w} p_0^2 \beta}{3 \varepsilon_0}. \quad (55)$$

Comparison between the space dependence of the relative permittivity within the GI equation and within its limiting LB equation for  $\gamma \rightarrow 1$  and  $n \rightarrow 1$  shows that consideration of the cavity field and electronic polarizability of water molecules makes the reduction of the permittivity of the electrolyte solution near the charged surface stronger in the case of the GI equation. More importantly, in the LB equation the value  $p_0 = 4.79 \text{ D}$  [63,64,68] (similarly as in the LPB model [16,42]) should be used in order to get  $\varepsilon_r(x \rightarrow \infty) = 78.5$ .

#### 4.3. Bikerman equation

In the limit of  $p_0 \rightarrow 0$  the particle distribution functions (Eqs. (52), (53) and (54)) transform into the Bikerman distribution functions [3,25–28,31,69,70]:

$$n_+(x) = \frac{n_0 n_s}{n_{0w}} \frac{e^{-e_0 \phi \beta}}{1 + (2n_0/n_{0w}) \cosh(e_0 \phi \beta)}, \quad (56)$$

$$n_-(x) = \frac{n_0 n_s}{n_{0w}} \frac{e^{e_0 \phi \beta}}{1 + (2n_0/n_{0w}) \cosh(e_0 \phi \beta)}, \quad (57)$$

$$n_w(x) = \frac{n_s}{1 + (2n_0/n_{0w}) \cosh(e_0 \phi \beta)}, \quad (58)$$

while Eq. (48) transforms into the Bikerman equation [3,25–28,31,69,70]:

$$\varepsilon_0 \varepsilon_{r,b} \frac{d^2 \phi}{dx^2} = 2 e_0 n_s n_0 \frac{\sinh(e_0 \phi \beta)}{\mathcal{H}(\phi, E)}, \quad (59)$$

where we transformed  $\varepsilon_0 \rightarrow \varepsilon_{r,b} \varepsilon_0$  with  $\varepsilon_{r,b} = 78.5$ , while  $\rho_{free}(x)$  is defined by Eq. (49). Eq. (56) predicts a Fermi–Dirac-like distribution for counterions if the lattice constant  $a$  is large enough. For higher values of the surface charge density ( $|\sigma|$ ), the counter-ion density saturates near the charged surface to its close packing value, while the well-known GC model [12,17,18] predicts unreasonably high values beyond the close-packing values (see also [3,25,70]).

#### 4.4. Limiting Poisson–Boltzmann equation

In the limit of very dilute solution everywhere in the electrolyte solution:

$$\sum_{j=+,-} n_j(x) \ll n_w(x), \quad (60)$$

and by taking into account the approximation  $n_{0w} \simeq n_s$ , we can neglect the second term in the denominator of Eqs. (56) and (57), so the particle distribution functions (Eqs. (56) and (57)) transform into Boltzmann distribution functions within the GC model [2,4,12,17,18,58]:

$$n_+(x) = n_0 e^{-e_0 \phi \beta}, \quad (61)$$

$$n_-(x) = n_0 e^{e_0 \phi \beta}, \quad (62)$$

while the number density of water molecules (Eq. (58)) becomes constant [3,70]:

$$n_w(x) = n_{0w}. \quad (63)$$

The Bikerman equation (Eq. (59)) transforms into the Poisson–Boltzmann equation (Eq. (21)) within GC model [12,17,18]:

$$\varepsilon_0 \varepsilon_{r,b} \frac{d^2 \phi}{dx^2} = 2 e_0 n_0 \sinh(e_0 \phi \beta). \quad (64)$$

#### 4.5. Osmotic pressure

Following a similar procedure (presented in Section 3.4) in the derivation of Eqs. (24) and (29), we multiply the LB equation (Eq. (48)) by  $\phi'$  and then integrate it [11,47,63] to get an expression for the osmotic pressure in the form:

$$\Pi_{LB} = -\frac{1}{2} \varepsilon_0 E(x)^2 - \frac{n_s}{\beta} \ln \left( \frac{n_s}{\mathcal{H}(\phi, E)} \right) - n_w(x) p_0 E(x) \mathcal{L}(p_0 E(x) \beta). \quad (65)$$

where  $\mathcal{H}(\phi, E)$  is defined by Eq. (51) and the number density of water  $n_w(x)$  by Eq. (54).

For small  $p_0 E(x) \beta$  and  $e_0 \phi \beta$  we can expand the 2nd and 3rd terms in Eq. (65) into Taylor series to get:

$$\Pi_{LB} \approx -\frac{1}{2} \varepsilon_0 \left( 1 + \frac{n_{0w} p_0^2 \beta}{3 \varepsilon_0} \right) E(x)^2 + \frac{2 n_0}{\beta} (\cosh(e_0 \phi(x) \beta) - 1). \quad (66)$$

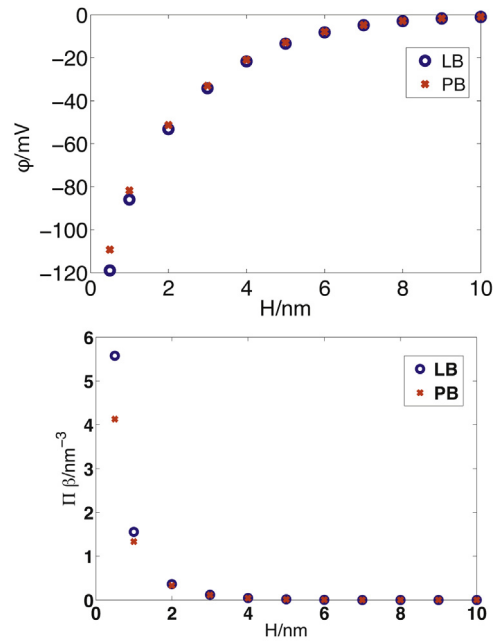


**Fig. 10.** Electric potential  $\phi(x=H/2)$  (upper panel) and osmotic pressure  $\Pi\beta$  (lower panel) between two negatively charged surfaces, calculated within the PB model (Eq. (31)) (saltires) and the LB model (Eq. (70)) (empty circles) as a function of the distance between charged surfaces ( $H$ ) (see Fig. 1) for a bulk salt concentration  $n_0/N_A = 0.1$  mol/l. Other model parameters are:  $\sigma_1 = -0.3$  As/m<sup>2</sup>,  $T = 298$  K, concentration of water  $n_{0w}/N_A = 55$  mol/l and dipole moment of water  $p_0 = 4.79$  Debye, where  $N_A$  is the Avogadro number.

Taking into account Eq. (55) above, Eq. (66) attains the PB form of the equation for osmotic pressure:

$$\Pi_{PB} = -\frac{1}{2} \varepsilon_0 \varepsilon_{r,b} E(x)^2 + \frac{2 n_0}{\beta} (\cosh(e_0 \phi(x) \beta) - 1). \quad (67)$$

In thermodynamic equilibrium the value of the osmotic pressure is equal everywhere in the space between the two charged surfaces (Fig. 1). In the case of like-charged surfaces where  $\sigma_1$  (at  $x=0$ ) and  $\sigma_2$  (at  $x=H$ ) are both negative or positive and equal ( $\sigma_1 = \sigma_2$ ), the electric field strength at  $x=H/2$  is zero, therefore the expression for osmotic pressure within the LB model (Eq. (65)) in the special case of  $\sigma_1 = \sigma_2$  simplifies to:

$$\begin{aligned} \Pi_{LB}(x=H/2) &= \frac{n_s}{\beta} \ln \left( \frac{n_{0w}}{n_s} \left( 2 \frac{n_0}{n_{0w}} \cosh(e_0 \phi_{LB}(x=H/2) \beta) + 1 \right) \right), \end{aligned} \quad (68)$$

where  $\phi_{LB}(x=H/2)$  is calculated from LB equation. Adopting the approximation  $(n_s/\beta) \ln(n_{0w}/n_s) = (n_s/\beta) \ln((n_s - 2n_0)/n_s) = (n_s/\beta) \ln(1 - 2n_0/n_s) \simeq -2n_0/\beta$  Eq. (68) transforms into:

$$\begin{aligned} \Pi_{LB}(x=H/2) &= -\frac{2 n_0}{\beta} + \frac{n_s}{\beta} \ln \left( 2 \frac{n_0}{n_{0w}} \cosh(e_0 \phi_{LB}(x=H/2) \beta) + 1 \right). \end{aligned} \quad (69)$$

For  $2(n_0/n_{0w}) \cosh(e_0 \phi_{LB}(x=H/2) \beta) \ll 1$  Eq. (68) can be further simplified to get:

$$\Pi_{LB}(x=H/2) = \frac{2 n_0}{\beta} (\cosh(e_0 \phi_{LB}(x=H/2) \beta) - 1). \quad (70)$$

In order to shed light on the influence of water polarization and the finite size of molecules on the osmotic pressure in an electrolyte solution confined by two charged surfaces, we compared it within the PB model and the LB model calculated at  $x=H/2$  using Eqs. (31) and (70), respectively (Fig. 10). Since in Eqs. (31) and (70) the electric potential at  $x=H/2$  is the only input data, Fig. 10 shows the

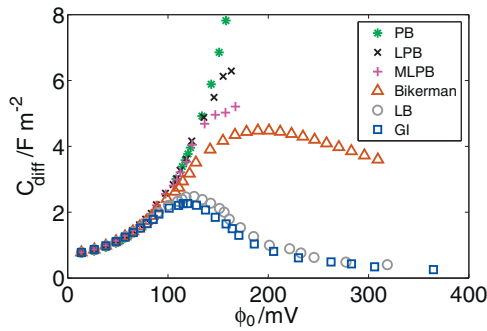


**Fig. 11.** Differential capacitance as a function of the surface potential  $\phi_0$  using Gouy–Chapman Eq. (72) (PB), LPB, MLPB, Bikerman, LB and GI model.

corresponding values of  $\phi(x=H/2)$  in the PB and LB models. We can see that the osmotic pressure within the like-charged surfaces as a function of the decreasing separation between the surfaces ( $H$ ) increases more in the LB than in the PB model. The difference between the predictions of the two models is much more significant for small separations  $H < 2$  nm, where the influence of water ordering and the excluded volume effect in the LB model becomes important.

## 5. Differential capacitance

To ascertain whether the described LB mean-field approach which includes the orientational ordering of water, the cavity field, the electronic polarizability of water and the finite size of molecules has improved the agreement between theory and experiments with respect to the classical GC model and the Bikerman model, one should compare the measured and predicted values of electric potential and differential capacitance of the EDL in both models. Using the GI equation, the predicted values of the electric potential at higher surface charge densities  $\sigma$  are substantially more negative than the corresponding values within the GC model using the PB equation or Bikerman equation (see also [71,72] and references therein).

Within the GC model, we can estimate the electric potential  $\phi_0$  at the surface (of an electrode for example) by applying the Grahame equation [5]:

$$\sigma = \sqrt{\frac{8 n_0 \varepsilon_0 \varepsilon_r}{\beta}} \cdot \sinh\left(\frac{e_0 \beta \phi_0}{2}\right), \quad (71)$$

where  $\phi_0$  is the surface potential, i.e.  $\phi(x=0)$ . The corresponding GC differential capacitance is [5,72]:

$$C_{GC} = \frac{d\sigma}{d\phi_0} = \sqrt{2 e_0^2 \beta n_0 \varepsilon_0 \varepsilon_r} \cdot \cosh\left(\frac{e_0 \beta \phi_0}{2}\right). \quad (72)$$

The GC model provides relatively good predictions for monovalent salts at concentrations below 0.2 mol/l in aqueous solutions and magnitudes of the surface potentials between 50 and 80 mV [5].

As can be seen in Fig. 11, the GC differential capacitance  $C_{GC}$  monotonously increases as a function of the increasing surface potential  $\phi_0$ . On the contrary, the differential capacitances calculated by the Bikerman, LB and GI equations start to decrease after reaching a maximal value, as shown in Fig. 11. At high  $\phi_0$  values the calculated LB and GI differential capacitances drop to very small values of the order of magnitude of 10 F/m<sup>2</sup> and smaller, in accordance with the experimental results [71,72] (see also Refs. [5–7,20]). Comparison of the differential capacitance ( $C_{diff}$ ) calculated using the LB and GI equations shows that the GI equation predicts lower differential capacitances in the region of  $\phi_0$  values larger than 100 mV (Fig. 11). In the same region of  $\phi_0$  the values of

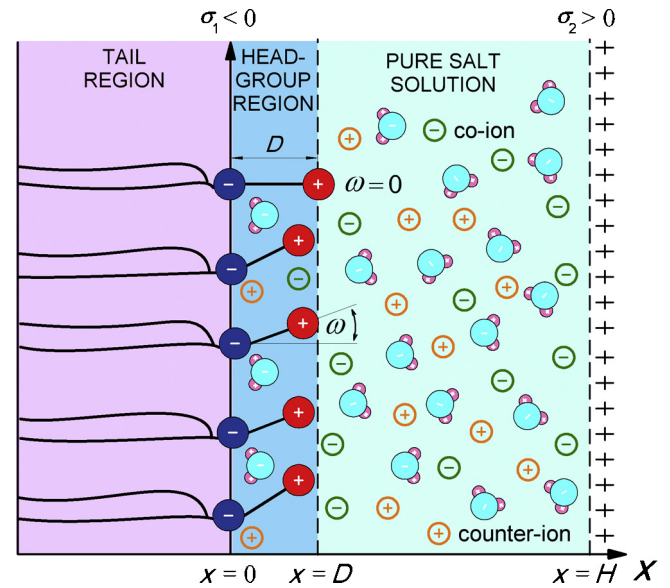


**Fig. 12.** Negative charges of dipolar (zwitterionic) lipid headgroups are described by a surface charge density  $\sigma_1$  at  $x=0$ . The positive charges of the headgroups of the dipolar lipids protrude into the electrolyte solution. Here  $D$  is the distance between the charges within a single dipolar lipid headgroup and  $\omega$  describes the orientational angle of the dipole within a single headgroup. The positive charge of an interacting nanoparticle (macroion) is described by a surface charge density  $\sigma_2$ .

$C_{diff}$  calculated using the Bikerman equation are much higher than LB and GI  $C_{diff}$ , and exceed the experimental values (see [71,72] and references therein).

The calculated dependences of  $C_{diff}(\phi_0)$  in Fig. 11 are presented only for positive values of  $\phi_0$ . The corresponding  $C_{diff}(\phi_0)$  curves for negative values of  $\phi_0$  are the mirror images of the  $C_{diff}(\phi_0)$  curves given in Fig. 11 (with respect to the vertical ( $\phi_0=0$ ) axis). The Bikerman, LB and GI  $C_{diff}(\phi_0)$  curves therefore have a so-called camel (or saddle-like) shape, as also observed experimentally [71,72], in Monte-Carlo simulations [73] and in molecular dynamic simulations [74].

Obviously, the GI equation can also be applied at higher surface charge densities (i.e. high voltage), where the classical PB equation within the GC model completely fails, as the differential capacitance  $C_{GC}$  (unlike the experimental results [72]) strongly and monotonously increases with increasing  $\phi_0$ , while in this region of  $\phi_0$  the Bikerman equation predicts too high values of  $C_{diff}$  (see Fig. 11). To conclude, the GI differential capacitance decreases with increasing  $\phi_0 > 0$  (after first reaching its maximum) and at large  $\phi_0$  attains the smallest values of all the models (Fig. 11), similar to that obtained experimentally.

Note that the predicted values of GI differential capacitance at high values of  $|\phi_0|$  are also smaller than the corresponding values of  $C_{diff}$  predicted by the empirical formula for  $\varepsilon(x)$  given in [7]. Moreover, if the GI equation is modified by taking into account the distance of closest approach for ions (see also [9,16,75]), the predicted values of  $C_{diff}$  would even closely approach the experimental values.

## 6. Dipolar surface in contact with an electrolyte solution within the modified Langevin–Poisson–Boltzmann model

### 6.1. Modified Langevin–Poisson–Boltzmann for a dipolar surface

In this section one of the flat surfaces that confines the electrolyte solution (as shown in Fig. 1) is replaced by a flat lipid layer composed of lipid molecules with zwitterionic dipolar headgroups (Fig. 12). Zwitterionic dipolar headgroups composed of a positively

charged trimethylammonium group and a negatively charged carboxyl group (at neutral pH) are described by two charges at a fixed distance  $D$  (Fig. 12). The negative charges of the phosphate groups of the dipolar (zwitterionic) lipids are described by a negative surface charge density  $\sigma_1$  at  $x=0$ ; the positive surface charge is distributed in the plane at  $x=H$  as in previous sections and described by surface charge density  $\sigma_2 > 0$ . The positively charged surface can, for example, be the surface of a charged nanoparticle (macroion) [65].

The corresponding Poisson's equation in planar geometry can be then written in the form [61]:

$$\frac{d}{dx} \left[ \varepsilon_0 \varepsilon_r(x) \frac{d\phi}{dx} \right] = 2 e_0 n_0 \sinh(e_0 \phi \beta) - \rho_{Zw}(x), \quad (73)$$

where  $\rho_{Zw}(x)$  is the macroscopic (net) volume charge density of the positive charges of the dipolar (zwitterionic) headgroups:

$$\rho_{Zw}(0 < x \leq D) = \frac{|\sigma_1| \mathcal{P}(x)}{D} \quad \text{and} \quad \rho_{Zw}(x > D) = 0, \quad (74)$$

$\mathcal{P}(x)$  is the probability density function indicating the probability that the positive charge of a dipolar lipid headgroup is located at the distance  $x$  from the negatively charged surface at  $x=0$ . Here the probability  $\mathcal{P}(x)$  is defined as [61]:

$$\mathcal{P}(x) = \Lambda \frac{\alpha \exp(-e_0 \phi(x) \beta)}{\alpha \exp(-e_0 \phi(x) \beta) + 1}, \quad (75)$$

where  $\Lambda$  is determined from the normalization condition

$$\frac{1}{D} \int_0^D \mathcal{P}(x) dx = 1. \quad (76)$$

The parameter  $\alpha$  is equal to the ratio between the average volume of the positively charged parts of dipolar (zwitterionic) headgroups and the average volume of the salt solution in the headgroup region. The boundary conditions are (see also [16,61]):

$$\frac{d\phi}{dx}(x=0) = -\frac{\sigma_1}{\varepsilon_0 \varepsilon_r(x=0)}, \quad (77)$$

$$\phi(x=D_-) = \phi(x=D_+), \quad (78)$$

$$\frac{d\phi}{dx}(x=D_-) = \frac{d\phi}{dx}(x=D_+), \quad (79)$$

$$\frac{d\phi}{dx}(x=H) = +\frac{\sigma_2}{\varepsilon_0 \varepsilon_r(x=H)}. \quad (80)$$

Fig. 13 shows the electric potential  $\phi$  and relative permittivity  $\varepsilon_r$  as a function of the distance from the negatively charged carboxyl groups at  $x=0$  (see Fig. 12). It can be seen in Fig. 13 that the relative permittivity  $\varepsilon_r(x)$  is considerably decreased within the lipid headgroup region. At the negatively charged plane of the carboxyl groups the value of  $\varepsilon_r(x)$  drops to 53 mV. The effect of the negatively charged plane of the carboxyl groups is already very weak at the distance  $x=D$ . Far away from the  $x=0$  surface the value of  $\varepsilon_r(x)$  is 78.5 mV.

## 6.2. Comparison with MD simulations

In recent years molecular dynamics (MD) simulations have given an insight into the interactions between the lipid membrane and the surrounding electrolyte [76–78]. The basis of the MD simulation method is the force field, which determines the behaviour of the studied system. AMBER, CHARMM and GROMOS, for example, are independent descriptions that are widely used for simulations of biological macromolecules. We constructed an MD model of the DPPC planar lipid bilayer in 450 mM KCl using the NAMD program and the all molecule performance CHARMM 36 force field. The model consists of 256 lipid units and 20174 water molecules. The

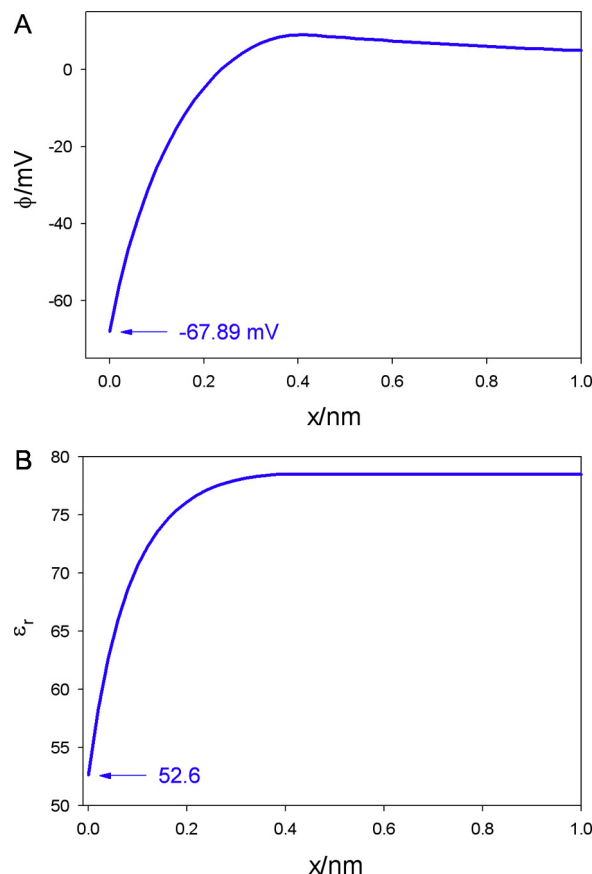


**Fig. 13.** Calculated electric potential  $\phi(x)$  (upper panel) and relative permittivity  $\varepsilon_r(x)$  (lower panel) as a function of the distance from the charged planar surface of negatively charged carboxyl groups at  $x=0$  (see Fig. 12) for large  $H$ . The model parameters are:  $\sigma_1 = -0.3 \text{ As/m}^2$ ,  $T = 298 \text{ K}$ ,  $p_0 = 3.1 \text{ Debye}$ ,  $D = 0.42 \text{ nm}$  bulk concentration of salt  $n_0/N_A = 0.1 \text{ mol/l}$ , concentration of water  $n_{0w}/N_A = 55 \text{ mol/l}$ , where  $N_A$  is the Avogadro number. The MLPB Eq. (73) was solved numerically as described in [61].

solvent was modelled by 153  $\text{K}^+$  and 153  $\text{Cl}^-$  ions [79,80]. Chemical bonds between hydrogen and heavy atoms were constrained to their equilibrium value. Long-range electrostatic forces were taken into account using a fast implementation of the particle mesh Ewald (PME) method [81,82]. The model was examined at constant pressure ( $1.013 \times 10^5 \text{ Pa}$ ) and constant temperature (323 K) employing Langevin dynamics and the Langevin piston method. The equations of motion were integrated using the multiple time-step algorithm. A time step of 2.0 fs was employed. Short- and long-range forces were calculated every first and second time steps, respectively. The model was equilibrated and followed for 30 ns. The last 15 ns of the simulation were used for extraction of the dipole orientation angle. From the positions of the P and N atoms the dipole was determined for all 256 lipids in each of 1500 simulation frames and exported to Matlab2012b. The distribution of the vector amplitude corresponding to distance  $D$  between the charges was extracted, as well as the distribution of the angle  $\omega$  between the dipole and the normal vector to the planar lipid bilayer plane (Fig. 12). To obtain the probability density  $\mathcal{P}(x)$ , the projection of each headgroup dipole on the normal vector to the planar lipid bilayer plane was calculated. The average distance between P and N atoms (0.42 nm) was used as a parameter  $D$  in the MLPB model (Eq. (73)).

A comparison between the probability density  $\mathcal{P}(x)$  calculated within the MLPB model (Eq. (75)) and  $\mathcal{P}(x)$  obtained in the MD simulations is presented in Fig. 14. Fig. 14 shows the space dependence of  $\mathcal{P}(x)$  calculated by using Eq. (75) for different values of the parameter  $\alpha$ . As can be seen in Fig. 14, the MLPB model predicts

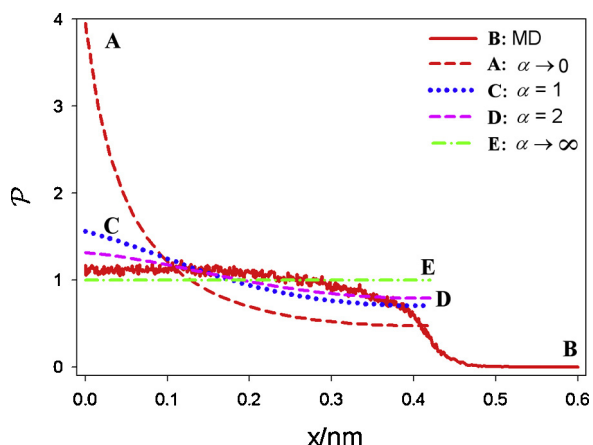


**Fig. 14.** Probability density  $\mathcal{P}(x)$  that the positive charge of the lipid dipolar headgroup (see also Fig. 12) is located at distance  $x$  from the negatively charged surface calculated by the MLPB model (A,C,D,E) and obtained from MD simulations (B) for  $\sigma_1 = -0.27$  As/m<sup>2</sup> and very large  $H$ . The values of MLPB model parameters are:  $T = 323$  K,  $p_0 = 3.1$  Debye,  $D = 0.42$  nm, bulk concentration of salt  $n_0/N_A = 0.1$  mol/l and the concentration of water  $n_{0w}/N_A = 55$  mol/l, where  $N_A$  is the Avogadro number. Adapted from [61].

saturation of the probability density function  $\mathcal{P}(x)$ , corresponding to close packing of the lipid headgroups in accordance with the results of the MD simulations.

It can therefore be concluded that taking into account the finite volume of the lipid headgroups leads to a better agreement between the predicted  $\mathcal{P}(x)$  dependences within the MLPB model and the MD simulations [61]. In the limit of  $\alpha \rightarrow \infty$  (when all lattice sites are occupied by headgroups) the probability density function  $\mathcal{P}(x)$  becomes constant as expected. On the other hand, in the limit of small values of  $\alpha$  (i.e. negligible volume of the headgroups) the probability density  $\mathcal{P}(x)$ , calculated using Eq. (75), approaches the probability density  $\mathcal{P}(x)$  determined by equation  $\mathcal{P}(x) = \Lambda \exp(-e_0\phi(x)\beta)$  (see also [61]). Fig. 15 shows the number densities of co-ions ( $n_-(x)$ ) and counter-ions ( $n_+(x)$ ) of the electrolyte solution in the vicinity and within the lipid headgroup region calculated within the MLPB model. For comparison, the spatial dependences of  $K^+$ ,  $Na^+$  and  $Cl^-$  determined within the MD simulation are also presented in the same figure. Ion number density profiles of the DPPC planar lipid bilayer in 450 mM KCl were calculated using the presented MD model, while ion number density profiles of the DOPC planar lipid bilayer in 1 M NaCl were kindly provided by Vacha et al. [83–85]. On comparison of  $n_-(x)$  and the spatially dependent number density of the  $Cl^-$  ion, qualitatively good agreement between the MLPB and both MD predictions can be observed in the region  $x > D$  and partially also in the region  $0 \leq x < D$ .

The depletion of negatively charged coions and  $Cl^-$  near the negatively charged surface at  $x = 0$  appears in both the MD model and in the MLPB model. The peaks in the number density of coions ( $n_-(x)$ ) and in the spatially dependent number density of  $Cl^-$  are predicted within the MD and MLPB models (Fig. 15). The peak in the number density of coions ( $n_-(x)$ ) obtained by the MLPB model is located at a distance  $D$ , close to the positive charges of the lipid dipolar headgroups, which is obviously due to the consideration that molecules of electrolyte solution are point-like particles. Both MD simulations showed a peak in the number density of  $Cl^-$  ions in the electrolyte solution nearby, but outside the region of the lipid headgroups. Regarding the number density of counter-ions ( $n_+(x)$ ) and the spatial dependence of  $Na^+$  and  $K^+$ , a difference in the predictions of the MD model and MLPB model can be observed in the vicinity of the phosphate groups at both sides of the  $x = 0$  plane (Fig. 15, lower panel). Unlike the predictions of the MLPB model, which shows strong accumulation of positively charged counter-ions, the results

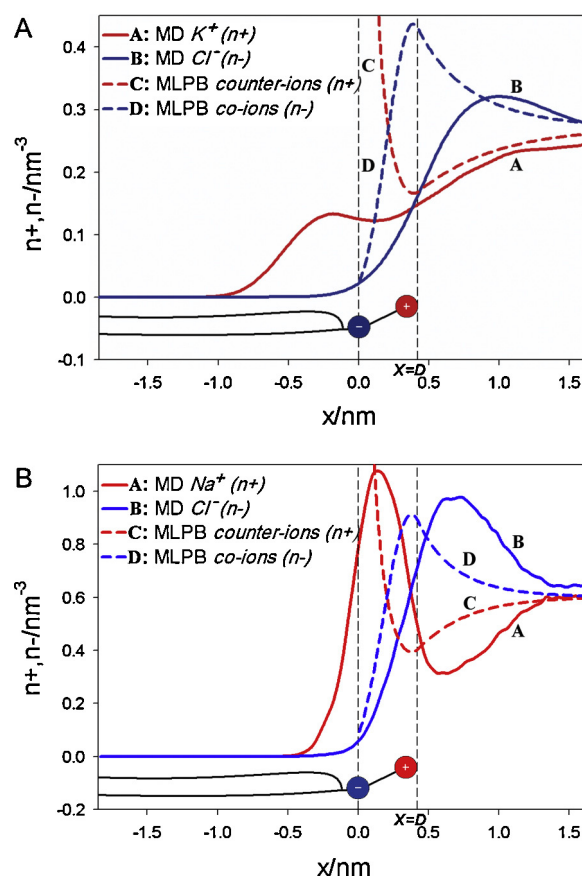


**Fig. 15.** The calculated number densities of coions ( $n_-$ ) and counterions ( $n_+$ ) in the electrolyte solution within the MLPB model (dashed lines) and MD simulations (full lines). Upper panel:  $\sigma_1 = -0.27$  As/m<sup>2</sup>,  $n_0/N_A = 0.45$  mol/l,  $T = 323$  K. The values of other parameters within the MLPB model are the same as in Fig. 13. Lower panel:  $\sigma_1 = -0.23$  As/m<sup>2</sup>,  $n_0/N_A = 1$  mol/l,  $T = 310$  K.

The MD results in the lower panel are adapted from [83].

of MD simulations exhibit a decrease of the number density of  $Na^+$  and  $K^+$ . The number density of  $K^+$  ions [83] is maximal in the electrolyte solution. It continuously decreases in the vicinity of the positive charges of the lipid dipolar headgroups. It exhibits a local peak at the distance  $x \approx -0.2$  nm which is already in the tail (hydrophobic) region. In the case of  $Na^+$  a strong maximum in number density appears at  $x \approx 0.2$  nm, i.e. in the region of the lipid headgroups (Fig. 15). Non-hydrated  $Na^+$  ions are smaller than  $K^+$  ions and therefore also accompanied by a larger ionic surface charge. This could be the reason that they probably penetrate rather deeply into the headgroup region and accumulate near the negative charges of the phosphate groups, while the larger (non-hydrated)  $K^+$  ions prefer to be located in the electrolyte solution. The difference in the number densities of  $Na^+$  and  $K^+$  in the MD model as shown in Fig. 15 (see also [83–85]) is not predicted in the MLPB model. In order to introduce this difference in  $Na^+$  and  $K^+$  number densities into the MLPB model, a different distance of closest approach for different cation species could be introduced in the MLPB model (see also [16]). The observed differences in the predictions of the MD and MLPB models in the vicinity of the  $x = 0$  charged plane partially spring from the fact that within the MLPB model the counterions are treated as point-like particles. Consideration of the finite-size of ions (described within the LB model in Section 4 of this review) would lead to better agreement between the predictions of the MD simulation and the results of theoretical modelling, i.e. lower values of  $(n_+(x=0))$  (see also Fig. 7). In addition, within the MD models  $Na^+$  and  $K^+$  ions may penetrate into the region of the hydrocarbon

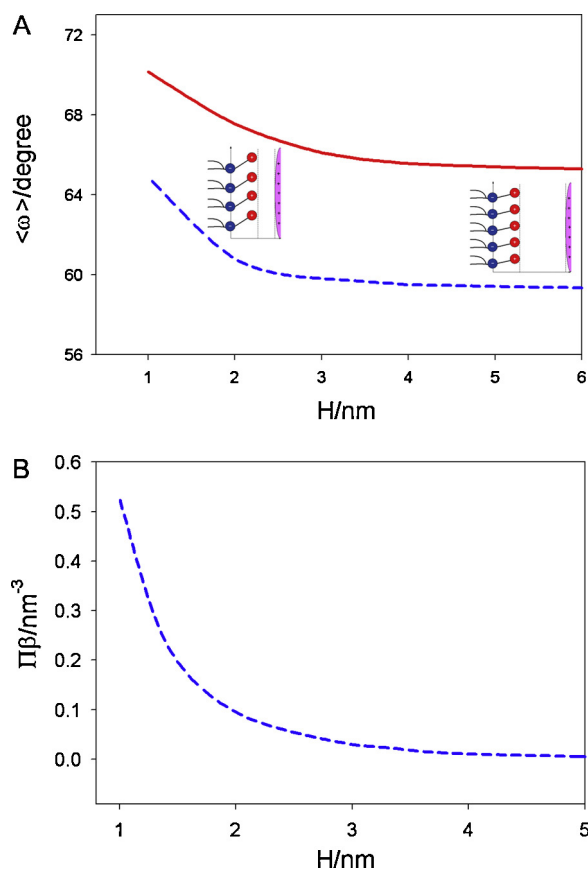


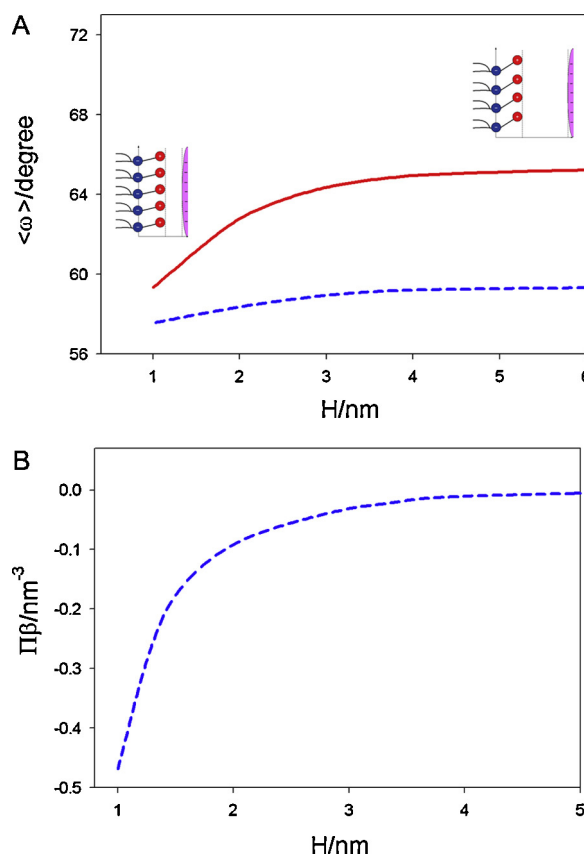
**Fig. 16.** Average lipid dipolar headgroup (zwitterionic) orientation angle ( $\omega$ ) (for definition see also Fig. 12) (upper panel) and osmotic pressure  $\Pi\beta$  (lower panel) between the dipolar headgroups and the positively charged surface of macroions as a function of the distance between the plane of the lipid phosphate groups and the surface of the macroion ( $H$ ) for two values of parameter  $\alpha$ : 0.5 (full line) and 5 (dotted line). The values of model parameters are:  $T=298$  K,  $\sigma_1 = -0.3$  As/m<sup>2</sup>, the dipole moment of water  $p_0 = 3.1$  Debye, bulk concentration of salt  $n_0/N_A = 0.1$  mol/l and concentration of water  $n_{0w}/N_A = 55$  mol/l.

Adapted from [65].

tails of lipid molecules  $x < 0$ , a feature which is not possible within the MLPB model since in the latter case the model boundary conditions prevent cations (as well as anions) from penetrating into the tail region of the lipid molecules  $x < 0$ . The predicted maxima and minima in the spatially dependent number densities of ions in the MD are broader and more shallow than those predicted in the MLPB model. This difference may spring from the thermal fluctuations of the lipid bilayer which are considered in MD simulations but not in the MLPB mean-field model. Far away from the charged planar surface, the number density of counter-ions equals the number density concentration of co-ions in the MD and MLPB models.

### 6.3. Average lipid dipolar headgroup orientation angle and osmotic pressure

Fig. 16 shows the influence of the approaching positively charged surface of a macroion to the surface of a zwitterionic (dipolar) lipid layer on the average orientation of the lipid headgroup orientation angle ( $\langle \omega \rangle$ ). As expected the value of  $\langle \omega \rangle$  increases with decreasing  $H$  due to electrostatic repulsion between the positively charged parts of the lipid headgroups and the positively charged macroion. Accordingly also the osmotic pressure between the headgroups and the positively charged macroion increases with decreasing  $H$ .



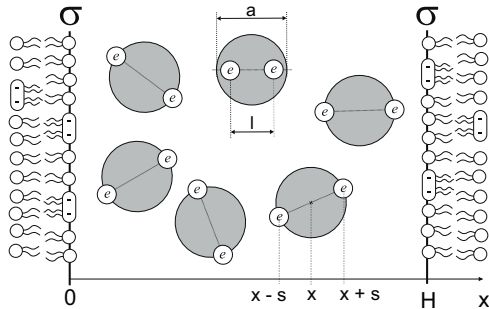
**Fig. 17.** (A) Average lipid dipolar (zwitterionic) headgroup orientation angle ( $\omega$ ) (for definition see also Fig. 12) and (B) osmotic pressure between the dipolar headgroups and negatively charged surface of macroion as a function of the distance between the plane of the lipid phosphate groups and the surface of macroion ( $H$ ) for two values of parameter  $\alpha$ : 0.5 (full line) and 5 (dotted line). The values of model parameters are:  $T=298$  K,  $\sigma_1 = -0.30$  As/m<sup>2</sup>, the dipole moment of water  $p_0 = 3.1$  Debye, bulk concentration of salt  $n_0/N_A = 0.1$  mol/l and concentration of water  $n_{0w}/N_A = 55$  mol/l.

Fig. 17 shows the influence of the approach of the negatively charged surface of a macroion on the average orientation of the lipid dipolar headgroup angle ( $\langle \omega \rangle$ ). Unlike the previous case presented in Fig. 14, the value of  $\langle \omega \rangle$  decreases with decreasing  $H$  due to electrostatic attraction between the positively charged parts of the lipid headgroups and the negatively charged surface of the macroion. Accordingly the osmotic pressure between the headgroups and the negatively charged macroion surface is also decreased with decreasing  $H$ .

## 7. Attraction between like-charged surfaces mediated by macroions with internal charge distribution

In biological systems charged membrane surfaces are surrounded by charged macromolecules, such as DNA and various proteins. Experiments with giant phospholipid vesicles indicated that certain charged plasma proteins [49,86] may induce the coalescence of like-charged lipid vesicles. In this section a mean-field theory is presented to explain the experimentally observed macroion-mediated attraction between like-charged lipid vesicles and other like-charged biological surfaces [87].

As shown in previous sections of this review, classical mean-field EDL theories always predict electrostatic repulsion between like-charged surfaces separated by a solution of dimensionless or finite-sized ions with a single point charge (Figs. 6 and 16) [4,11,47,58,88]. On the other hand, it was shown that the attraction between like-charged biological surfaces may be



**Fig. 18.** Schematic illustration of two negatively charged planar lipid bilayer surfaces with surface charge density  $\sigma$  separated by a solution containing spherical macroions (counterions) with spatially distributed positive charge. Large spheroidal multivalent macroions are modelled as spheres having average diameter  $a$ . The space charge distribution of the macroion is described by two effective poly-ions of charge  $e = Ze_0$  located at different well-separated positions (i.e. at a distance  $l \leq a$ ) [49]. The main axis of the macroion coincides with the line connecting the two poly-ions. In this particular study charges within a macroion are separated by a fixed distance  $l = a$ , where  $a$  is the diameter of the macroions.

explained by inter-ionic correlations, i.e. particle-particle correlations [57,89–92]. Additionally, other non-electrostatic forces can also contribute to the attraction between biological surfaces, such as van der Waals attraction forces [47], or forces of entropic nature such as oscillatory forces [4,93] or depletion forces [94–96] which become increasingly important in the strong coupling regime. Orientational ordering (intra-ionic correlation) of macroions with internal charge distribution may also lead to attractive forces between like-charged surfaces [49–51,97].

In this section a generalization of the mean-field theory of the EDL is presented by explicitly taking into account the internal space charge distribution [98] of multivalent spheroidal macroions (Fig. 18). Using mean-field density functional theory it is then shown that the orientational ordering of spheroidal macroions with internal charge distribution may give rise to attraction between neighbouring like-charged biological surfaces [49,99]. To assess the limitations of the described mean field theory its predictions are tested using Monte Carlo simulations.

### 7.1. Spheroidal macroions

In this model we describe two like-charged flat surfaces, each of area  $A$ , separated by a distance  $H$ . The charge distribution of both membrane surfaces is described by uniform surface charge density  $\sigma$  at  $x=0$  and  $x=H$  (Fig. 18). The space between the charged surfaces is filled with a solution of charged macromolecules of a single species (counterions). Charged macromolecules are treated in the most simple way as spheroidal macroions (Fig. 18) freely moving in the solution [49,99]. The spheroidal macroion is described as a sphere of diameter  $a$  (globular protein) within which two equal positive point charges, each of valency  $Z$  ( $e = Ze_0$ ), are separated by distance  $l = a$  (Fig. 18). The distance of closest approach of the spherical macroions to the charged surfaces is taken into account, while the direct particle-particle hard core interactions are completely ignored.

The charged spheroidal macroions are subject to positional and orientational degrees of freedom. For each macroion the centre of charge distribution (also its geometric centre) is located at  $x$  and  $n(x)$  is the corresponding number density of the macroions. The two point charges are located at geometrically opposite points on the surface of the sphere such that, when projected on to the  $x$ -axis, their positions are at  $x+s$  and  $x-s$  respectively, as shown in Fig. 18.

Taking into account that the two point charges of the macroions are indistinguishable, all possible orientations of the macroion can be described by values of  $s$  in the interval  $0 < s < l/2$  (see Fig. 18).

Therefore, the orientation of the spherical macroion is specified by the conditional probability  $p(s|x)$  which must satisfy the relation [58,99]:

$$\frac{2}{l} \int_0^{l/2} p(s|x) ds = 1, \quad (81)$$

where  $p(s|x) = 0$  for any  $x$  and  $|s| > l/2$ .

The equilibrium configuration of the system can be determined by minimizing the free energy. The free energy of the system per unit area is [49]:

$$\begin{aligned} \frac{F}{A} = kT \int_0^H dx [ \varepsilon_0 \varepsilon_{r,b} \phi'(x)^2 + [n(x) \ln(n(x) \nu_0) - n] \\ + n(x) \langle p(s|x) \ln p(s|x) \rangle ], \end{aligned} \quad (82)$$

where the first term is the electrostatic contribution to the free energy. The prime denotes the first derivative of the electric potential  $\phi$  with respect to  $x$ . The second term is the contribution due to configurational entropy [3,13,16], where  $\nu_0$  is the volume of a single lattice site. The third term denotes the contribution of orientational ordering of the macroions. The centres of the macroions are allowed to be distributed in the region  $l/2 \leq x \leq H - l/2$ , i.e. the distance of closest approach is taken into account to ensure that the spheroidal macroions are confined within the region defined by the charged walls. The average of an arbitrary function  $g(x)$  is defined as:

$$\langle g(x) \rangle = \frac{2}{l} \int_0^{l/2} g(x, s) ds. \quad (83)$$

In the following, the limits of integration in the free energy expression are extended to infinity in both directions:

$$\begin{aligned} \frac{F}{A} = kT \int_{-\infty}^{\infty} dx [ \varepsilon_0 \varepsilon_{r,b} \phi'(x)^2 + [n(x) \ln(n(x) \nu_0) - n] \\ + n(x) \langle p(s|x) \ln p(s|x) \rangle ], \end{aligned} \quad (84)$$

where the values of  $n(x)$  and  $\phi'(x)$  are assumed to be zero outside the space between the two charged surfaces.

The equilibrium state of the system is determined by the minimum of the total free energy  $F$ , subject to the constraints that (a) the orientational probability of the spheroidal charged macroions integrated over all possible projections (Eq. (81)) is equal to one, and that (b) the total number of charged macroions is conserved [3,49]. To solve this variational problem, a functional  $\int_{-\infty}^{\infty} \mathcal{F} dx$  is constructed:

$$\begin{aligned} \int_{-\infty}^{\infty} \mathcal{F} dx = \frac{F}{AkT} + \int_{-\infty}^{\infty} \lambda(x) n(x) \left( \frac{2}{l} \int_0^{l/2} p(s|x) ds - 1 \right) dx \\ + \mu \int_{-\infty}^{\infty} n(x) dx, \end{aligned} \quad (85)$$

where  $\lambda(x)$  and  $\mu$  are the local and global Lagrange multipliers, respectively.

Taking into account Eq. (84), we can rewrite Eq. (85) in the form:

$$\begin{aligned} \int_{-\infty}^{\infty} \mathcal{F} dx = \int_{-\infty}^{\infty} dx [ \varepsilon_0 \varepsilon_{r,b} \phi'(x)^2 / kT + n(x) \ln(n(x) \nu_0) \\ - n(x) + n(x) \langle p(s|x) \ln p(s|x) \rangle ] \\ + \int_{-\infty}^{\infty} dx n(x) \lambda(x) [ \langle p(s|x) \rangle - 1 ] + \mu \int_{-\infty}^{\infty} n(x) dx. \end{aligned} \quad (86)$$

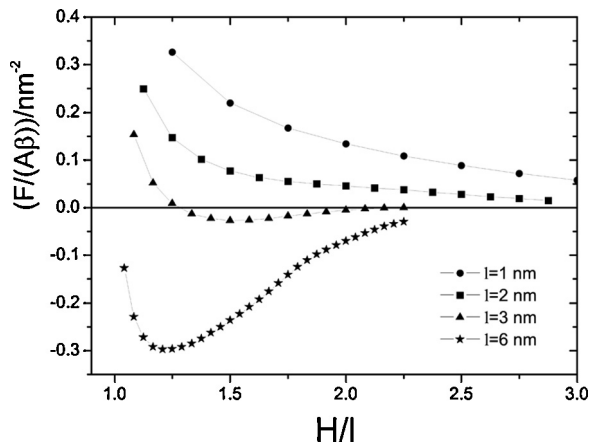


**Fig. 19.** The normalized free energy  $F/kT$  as a function of the distance between two negatively charged surfaces  $H$  calculated for four different extensions between charges  $l$  within the charged macroions. Other model parameters are  $Z=1$ ,  $\sigma = -0.033 \text{ As/m}^2$  and  $l_b = 0.7 \text{ nm}$  (adapted from [49]). The hard core interaction between the macroions and charged walls is taken into account by means of the distance of closest approach ( $l/2$ ), while the hard core interaction between charged macroions is not considered.

In equilibrium, the first variation of the functional  $\int_{-\infty}^{\infty} \mathcal{F} dx$  should be zero which, after some rearrangements, yields the equation for the number density [49]:

$$n(x) = \frac{e^{-\mu}}{\nu_0} (e^{-Z e_0 \beta \phi(x+s)} - Z e_0 \beta \phi(x-s)) \quad (87)$$

and the volume charge density [49]:

$$\rho(x) = \frac{2Ze_0}{\nu_0} (e^{-Z e_0 \beta \phi(x)} - Z e_0 \beta \phi(x+2s) - \mu). \quad (88)$$

The averaging is performed over  $s$ . The derived expression Eq. (88) for the volume charge density  $\rho(x)$  and the Poisson equation yield the integro-differential equation for the reduced electric potential in the form [49]:

$$\phi''(x) = -\frac{2Ze_0}{\epsilon_0 \epsilon_{r,b} \nu_0} (e^{-Z e_0 \beta \phi(x)} - Z e_0 \beta \phi(x+2s) - \mu). \quad (89)$$

The boundary conditions for Eq. (89) at the two charged surfaces  $x=0$  and  $x=H$  are:

$$\phi'(x=0) = -\frac{\sigma}{\epsilon_0 \epsilon_{r,b}}, \quad \phi'(x=H) = \frac{\sigma}{\epsilon_0 \epsilon_{r,b}}. \quad (90)$$

In this theoretical model, the finite size of the charged macroions is taken into account only by considering the distance of closest approach of the centre of the macroions to the charged surface ( $l/2$ ). Eq. (89) was solved numerically as described in [49]. The solution of the integro-differential Eq. (89) yields the equilibrium potential  $\phi(x)$ , and the corresponding equilibrium distribution  $n(x)$  and probability density  $p(s|x)$ . When the charged macroions are *uniformly* distributed between the charged surfaces, the free energy is independent of the distance between the charged surfaces and can therefore be taken as a reference value in determining the values of the equilibrium free energy [3,49]. Fig. 19 shows the electrostatic free energy (Eq. (84)) as a function of the distance between the two negatively charged surfaces for different distances between the charges within a single macroion (see also Fig. 18). For small surface charge density  $|\sigma|$  and small separation between the charges within the charged macroion, the interaction was found to be repulsive for all distances between the charged surfaces [49]. However, large enough  $|\sigma|$  and  $l$  yield non-monotonous behaviour of the free energy  $f$  with a minimum representing the equilibrium distance between the charged membrane surfaces (Fig. 19).

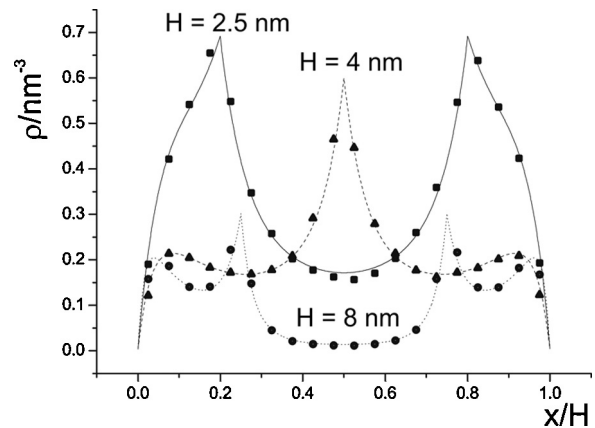


**Fig. 20.** Profile of the volume charge density due to positively charged divalent macroions ( $Z=1$ ) between two negatively charged surfaces. Lines represent the solutions of the integro-differential Eq. (89), points represent results of the Monte Carlo simulations. Model parameters:  $l=2 \text{ nm}$ ,  $\sigma = -0.07 \text{ As/m}^2$ . The hard core interaction between the macroions and charged walls is taken into account by means of the distance of closest approach ( $l/2$ ), while the hard core interaction between charged macroions is not considered. Adapted from [49].

We now discuss a comparison of the results obtained from the above presented theoretical analysis and Monte Carlo (MC) simulations. The results of solving the integro-differential Eq. (89) and the results of Monte-Carlo simulation were shown to be in excellent agreement [49,99]. Monte Carlo simulations are widely used to describe solutions of point-like ions [58,100,101], finite-sized ions [102–104], or ions with internal charge distribution [49–51,99] in contact with charged surface(s). In the MC simulation presented in this section, the standard MC Metropolis algorithm [105] with Lekner periodic boundary conditions [106] in directions parallel to the charged walls was used [49,99]. In each MC step, a spherical macroion is chosen at random to be rotated around its centre or linearly displaced [105] as described in [49,99]. Computation of the potential in a periodic system with 2-D symmetry is performed by the Lekner–Sperb method [101,106,107], which is an alternative to the Ewald summation [108].

Fig. 20 shows the results obtained from solutions of the integro-differential equation and MC simulations for the volume charge density  $\rho(x)$  in an aqueous solution of divalent charged spherical macroions ( $Z=1$ ) confined between two negatively charged planar surfaces separated by a distance  $H$ . The excellent agreement between the calculated volume charge density profiles (curves) and the results of Monte Carlo simulations (points) is evident [49,99]. For a value of  $H$  which is comparable to the separation of charges within a single charged macroion ( $l$ ), i.e. for  $H=2.5 \text{ nm}$  (squares), the charge density profile in the solution exhibits a single peak at each side, indicating that the macroions (on the average) orient to form electrostatic bridging between the two charged planar surfaces. On the other hand, for somewhat larger distances ( $H=4 \text{ nm}$ ) between the charged surfaces, we see a peak in the middle (triangles), which corresponds to partial overlapping of the ordered macroions in the middle of the space between the two like-charged surfaces (see Fig. 21). The charges on the macroions of both layers contribute to  $\rho(x)$  at  $x=H/2$ , so a central peak in the volume charge density  $\rho(x)$  is formed. For even larger distances ( $H=8 \text{ nm}$ ), the profile exhibits twin-peaks close to the two charged surfaces due to orientational ordering of the macroions, with one charge close to the charged surface.

The concept of a free energy decrease due to orientational ordering we previously used in determination of the equilibrium shapes of phospholipid bilayers (Refs. [109–111]), where it was shown that the in-plane orientational ordering of anisotropic membrane

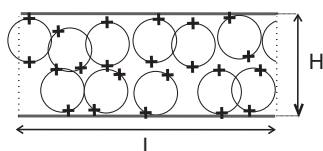


**Fig. 21.** Schematic representation of spherical divalent macroion positions and orientations at distance  $H \approx 4$  nm, where the diameter of the macroion is  $l = 2$  nm. At the distance  $H = 4$  nm, a peak in the density distribution of charges appears in the middle between the surfaces, as seen in Fig. 20.

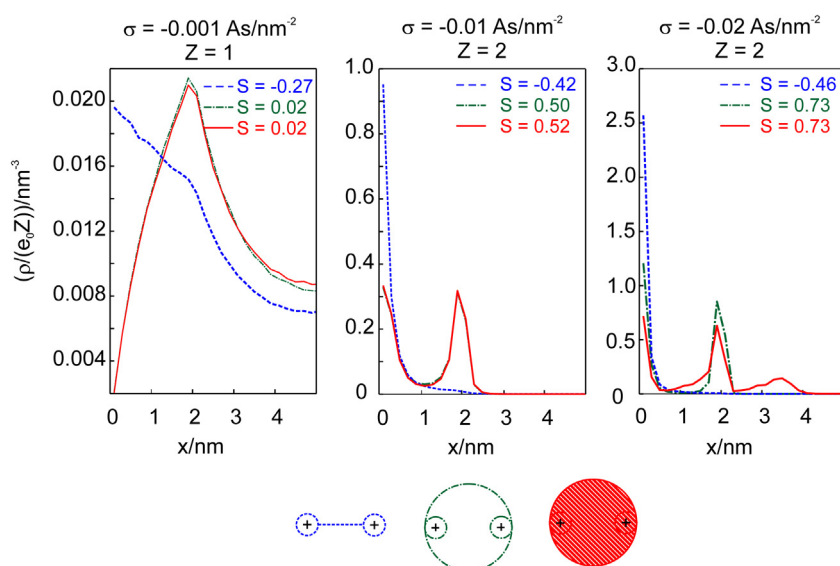
constituents can decrease the free energy of a phospholipid vesicle by stabilizing shapes with larger area regions having unequal principal membrane curvatures. The in-plane ordering of membrane components was later generalized to three-dimensional ordering of ions in the EDL [49,51,97]. The results presented in this section show that internal degrees of freedom (orientational and positional ordering of constrained charges), coupled with fixed distance imposed on pairs of charges within the macroions, may contribute to the decrease of the free energy of the system of spherical macroions confined between two charged surfaces. As shown in Fig. 19 the effect may be strong enough to cause an attractive interaction between the like-charged surfaces. This attractive interaction completely vanishes when the two charges within a single macroion are brought towards the centre of the ion, as happens in the standard GC theory, to which our equations reduce when the parameter  $l$  approaches zero [49].

Fig. 19 shows that the interaction between the charged surfaces changes from attractive to repulsive as the distance between the charges in a single charged macroion ( $l$ ) decreases at a fixed  $\sigma$ . This result indicates that the attraction between the like-charged surfaces presented in Fig. 19 originates from the imposed inter-charge interaction expressed by the fixed distance between the charges within a single macroion (Fig. 18), i.e. from intra-particle charge interactions.

## 7.2. Spheroidal and rod-like macroions

Another interesting feature of the problem of macroions as mediators of attractive interactions between like-charged surfaces is a comparison between the orientational ordering of spherical and rod-like macroions near charged surfaces and/or between charged surfaces. The origin of the bridging attraction in the system of spherical charged macroions with quadrupolar internal charge distribution (Fig. 19) [49,99] is identical to that in the system of rod-like charged macroions [50,51,97]; namely, the energetically favourable orientational ordering of the quadrupoles in the spatially varying electric field. A comparison of the orientational ordering of rod-like macroions, spherical macroions without hard core interactions between the macroions (overlapping of the macroions is allowed) and spherical macroions with hard core interactions between macroions (overlapping of the macroions is not allowed) is presented in Fig. 22. The volume charge distribution of rod-like and spherical positively charged quadrupolar macroions, confined in the space between two like-charged surfaces with separation  $H > 2l$ , was calculated using MC simulations for different values of the valency of the macroions ( $Z$ ) and different values of the surface charge density ( $\sigma$ ) of the negatively charged surfaces (Fig. 22).

The calculated volume charge distribution  $\rho(x)$  and the average order parameter  $S$  (Fig. 22) show distinctive differences in the average orientation of rod-like and spherical macroions near the charged surfaces for a distance between the two charged surfaces  $H = 10$  nm. It can be seen in Fig. 22 that for low values of the surface charge density ( $|\sigma|$ ) and small valency of the macroions ( $Z$ ), the rod-like macroions are not oriented in a direction orthogonal to the charged plates, but predominantly in a direction parallel to the charged surfaces, i.e. they are predominantly attached to the two charged planar surfaces (see also Fig. 23). Accordingly, the distribution peak of the volume charge density of the rod-like macroions is located at  $x = 0$  (the other one at  $x = H$ ). On the other hand, for higher values of ( $|\sigma|$ ) and  $Z$  both kinds of spherical macroions are predominantly oriented orthogonally to the charged surface and



**Fig. 22.** Volume charge distribution between two charged surfaces for three different kinds of macroions: rod-like macroions (blue), spherical macroions without a hard core interaction between the macroions (green), and spherical macroions with a hard core interaction between the macroions effect (red), predicted by MC simulation for  $H = 10$  nm,  $l = 2$  nm and different valency of the macroions ( $Z$ ) and different surface charge density ( $\sigma$ ). Because of symmetry, only half of the space between the two charged surfaces is plotted.  $H = 10$  nm,  $l = 2$  nm. The nematic order parameter  $S$  is defined as  $S = ((3 \cos^2(\vartheta) - 1)/2)$ , where the angle  $\vartheta$  describes the orientation of the axis connecting the two charges of the nanoparticle with respect to the  $x$  axis.  $S = 0$  means that the nanoparticles are not oriented, while  $S = 1$  corresponds to the nanoparticles being fully oriented with respect to the  $x$ -axis. The hard core interaction between the macroions and charged walls is taken into account by means of the distance of closest approach ( $l/2$ ).

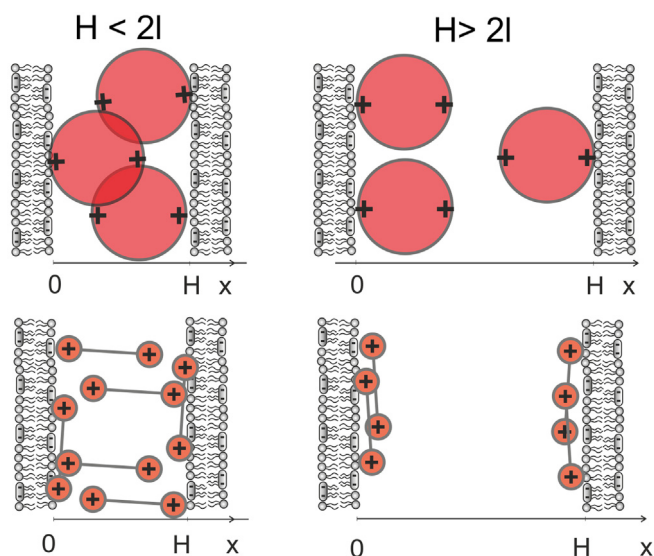


**Fig. 23.** Schematic figure representing the different orientational ordering of rod-like and spherical macroions at large and small distance between two like-charged surfaces. Due to their stronger average orientation in the orthogonal direction spherical macroions are better mediators of attractive interactions between like-charged surfaces than rod-like macroions.

therefore exhibit two peaks in their volume charge distribution. The excluded volume effect (i.e. hard core interactions between spherical macroions) is important only in the third case for  $Z=2$  and  $\sigma = -0.02 \text{ As/m}^2$ , i.e. in the stronger coupling regime. In the third (extreme right) panel of Fig. 22 it can also be seen that considering hard core interactions between the macroions results in the appearance of the third peak in the volume charge distribution of the spherical macroions as the consequence of the exclusion volume effect. Namely, in this case the spherical macroions close to the charged surface completely fill the space in the first row (saturation) and the rest of them are forced to find the energetically most favourable location further away from the charged surface. Nevertheless, the average order parameter of the spherical macroions is the same if we take into account the hard core interactions between macroions or not.

The average orientation of macroions in the solution between two like-charged surfaces may have a strong influence on the system's free energy and consequently also on the attractive/repulsive interaction between like-charged surfaces as indicated in [49–51,99]. Stronger orientation of the macroions in the orthogonal direction with respect to the charged surface contributes to stronger attraction between the like-charged surfaces. Based on the results presented in [10,49,112], Fig. 23 shows schematically the difference in orientational ordering between rod-like and spherical macroions for different distances between the two like-charged surfaces ( $H$ ). For small  $H$  ( $l < H < 2l$ ) some of the rod-like macroions are oriented orthogonally to the charged surfaces and some in a direction parallel to the charged surfaces (Fig. 23). On the other hand, for larger  $H$  ( $H > 2l$ ) all rod-like macroions are oriented in a direction parallel to the charged surfaces (Fig. 23). In accordance with our observation, a rod-like macroion-mediated attractive interaction between two like-charged surfaces was predicted in the range  $l < H < 2l$ , but not in the range  $H > 2l$  [50].

On the other hand, at high enough ( $|\sigma|$ ) and  $Z$  spherical macroions are mostly oriented orthogonally even for higher surface separations  $H > 2l$  (Fig. 23) leading to the conclusion that spherical macroions are better mediators of attractive interactions between like-charged surfaces than rod-like macroions (see also [49–51,99]).

To conclude, it is shown in this section that the density functional theory described (which does not include direct interactions between macroions) and the Monte Carlo simulation (which in contrast does include direct interactions between macroions) show remarkably good agreement between their predictions (Fig. 20). We may thus conclude that the bridging effect arising from the orientational ordering of macroions with internal charge distribution may explain the observed attractive interaction between like-charged surfaces [49–51,99]. Direct interaction between charged macroions may give rise to additional effects.

## 8. Conclusions

The results presented in this review provide an interesting perspective on the importance of modelling the relative permittivity in understanding EDL phenomena. A key feature that contributes to better agreement between theory and experiment is the inclusion of space-dependent permittivity, which is in general a function of the electric potential and electric field. Analytical expressions for its space dependence are derived within both models, i.e. within the LPB and LB models. Importantly, the EDL models presented in this work take into account the excluded-volume effect, orientational ordering of water in the saturation regime, the electronic polarizability of water and the concept of the cavity field. All these enable us to understand the mechanisms responsible for the spatial dependence of permittivity.

As an example of the application of the EDL models described, we calculated the differential capacitance of a charged surface in contact with an electrolyte solution as a function of the surface potential within the MLB model. Unlike the prediction of classical GC theory where the differential capacitance is a monotonous increasing function of the surface potential, in the MLB model, after reaching its maximal value, the differential capacitance decreases with increasing surface potential in accordance with experimental results. As another possible application we presented a model of a zwitterionic lipid surface in contact with an electrolyte solution of monovalent salt ions and water dipoles. It was shown that the permittivity in the zwitterionic headgroup region is decreased, while the corresponding electric potential becomes strongly negative.

The osmotic pressure of an electrolyte solution between a zwitterionic lipid surface and a charged particle (macroion) was also considered theoretically. It was indicated that in the close vicinity of the positively charged macroion the zwitterionic lipid headgroups are less extended in the direction orthogonal to the membrane surface, which coincides with the increase of osmotic pressure between the lipid surface and the macroion. In the case of a negatively charged macroion the effect is the opposite, i.e. the zwitterionic lipid headgroups are more extended, while the osmotic pressure between the lipid surface and the macroion is decreased.

Using the LPB and LB model equations described predicts that the attractive interaction between like-charged surfaces with an intermediate solution of monovalent ions is always repulsive. Therefore we hypothesized that the charged particles with a quadrupolar internal charge distribution may act as mediators, resulting in attraction between the like-charged surfaces. The above hypothesis was proved within the density functional theory (which is a mean field approach) and also by using Monte Carlo (MC) simulations. A remarkably a good agreement between the predictions of both methods was demonstrated.

Nowadays, numerical simulations provide a new window into the theoretical description of different physical phenomena where analytical solutions do not exist. The sophistication of the GC model and its PB equation allowed us to include additional properties of

the EDL, in an attempt to better characterize its complex behaviour; this would not be possible without the use of numerical simulations which were crucial in the validation of the models with high surface charge density regimes. Some of the predictions of the EDL mean-field theoretical considerations were also evaluated by molecular dynamics (MD) simulation and Monte Carlo (MC) simulations.

But finally there still remains the question of which important physical properties of the EDL are not yet considered in existing theoretical models of the EDL. This formidable task and further refinement and understanding of EDL behaviour remain the long-term goal.

## Acknowledgements

This work was supported by Slovenian Research Agency (ARRS) grants J3-2120, J1-4109, J1-4136, J3-4108 and P2-0232. A.V. was also supported by the European Social Fund and SMARTEH. P.B.S., and E.G. partially by a grant from the Slovenian Human Resources Development and Scholarship Fund.

## References

- [1] S.W. Kenkel, J.R. Macdonald, A lattice model for the electrical double layer using finite-length dipoles, *Journal of Chemical Physics* 81 (1984) 3215–3222.
- [2] G. Cevc, Membrane electrostatics, *Biochimica et Biophysica Acta* 1031 (3) (1990) 311–382.
- [3] V. Kralj-Iglič, A. Iglič, A simple statistical mechanical approach to the free energy of the electric double layer including the excluded volume effect, *Journal of Physics II* (1996) 477–491.
- [4] J.N. Israelachvili, *Intermolecular and Surface Forces*, Academic Press, London, 1997.
- [5] H.J. Butt, K. Graf, M. Kappl, *Physics and Chemistry of Interfaces*, Wiley-VCH, Weinheim, 2003.
- [6] A.A. Kornyshev, Double-layer in ionic liquids: paradigm change? *Chemical Physics Letters* 111 (2007) 5545–5557.
- [7] M. Bazant, M. Kilic, B. Storey, A. Ajdari, Towards an understanding of induced-charge electrokinetics at large applied voltages in concentrated solutions, *Advances in Colloid and Interface Science* 152 (2009) 48–88.
- [8] Z. Arsov, M. Rappolt, J. Grdodolnik, Weakened hydrogen bonds in water confined between lipid bilayers: the existence of a long-range attractive hydration force, *ChemPhysChem* 10 (9) (2009) 1438–1441.
- [9] T. Nagy, D. Henderson, D. Boda, Simulation of an electrical double layer model with a low dielectric layer between the electrode and the electrolyte, *Journal of Physical Chemistry B* (2011) 11409–11419.
- [10] D. Kabaso, E. Gongadze, Š. Perutkova, V. Kralj-Iglič, C. Mateschegewski, U. Beck, U. van Rienen, A. Iglič, Mechanics and electrostatics of the interactions between osteoblasts and titanium surface, *Computer Methods in Biomechanics and Biomedical Engineering* 14 (5) (2011) 469–482.
- [11] R. Misra, S. Das, S. Mitra, Electric double layer force between charged surfaces: effect of solvent polarization, *Journal of Chemical Physics* 138 (2013) 114703.
- [12] S. McLaughlin, The electrostatic properties of membranes, *Annual Review of Biophysics and Biophysical Chemistry* 18 (1989) 113–136.
- [13] A. Safra, *Statistical Thermodynamics of Surfaces, Interfaces, and Membranes*, Addison-Wesley Publishing Company, 1994.
- [14] C.W. Outhwaite, A treatment of solvent effect in the potential theory of electrolyte solution, *Molecular Physics* 31 (5) (1976) 1345–1357.
- [15] C.W. Outhwaite, Towards a mean electrostatic potential treatment of an ion-dipole mixture or a dipolar system next to a plane wall, *Molecular Physics* 48 (3) (1983) 599–614.
- [16] E. Gongadze, U. van Rienen, V. Kralj-Iglič, A. Iglič, Spatial variation of permittivity of an electrolyte solution in contact with a charged metal surface: a mini review, *Computer Methods in Biomechanics and Biomedical Engineering* 16 (2013) 463–480.
- [17] M.G. Gouy, Sur la constitution de la charge électrique à la surface d'un électrolyte, *Journal de Physique et Le Radium* (1910) 457–468.
- [18] D.L. Chapman, A contribution to the theory of electrocapillarity, *Philosophical Magazine* 6 (1913) 475–481.
- [19] R. Heinrich, M. Gaestel, R. Glaser, The electric potential profile across the erythrocyte membrane, *Journal of Theoretical Biology* 96 (1982) 211–231.
- [20] E. Gongadze, Influence of the surface structure of a biomaterial on the field distribution in the neighbouring biosystem, Dr. Ing. Thesis, University of Rostock, Rostock, 2011.
- [21] O. Stern, Zur theorie der elektrolytischen doppelschicht, *Zeitschrift für Elektrochemie* 30 (1924) 508–516.
- [22] H. Helmholtz, Studien über elektrische grenzschichten, *Annals of Physics* 243 (7) (1879) 337–382.
- [23] J.N. Israelachvili, H. Wennerstrom, Role of hydration and water structure in biological and colloidal interactions, *Nature* 379 (1996) 219–225.
- [24] E. Gongadze, U. van Rienen, A. Iglič, Generalized Stern models of an electric double layer considering the spatial variation of permittivity and finite size of ions in saturation regime, *Cellular and Molecular Biology Letters* 16 (2011) 576–594.
- [25] J. Bikerman, Structure and capacity of electrical double layer, *Philosophical Magazine* 33 (1942) 384–397.
- [26] T. Grimley, N. Mott, The contact between a solid and a liquid electrolyte, *Discussions of the Faraday Society* 1 (1947) 3–11.
- [27] T. Grimley, The contact between a solid and a liquid electrolyte, *Proceedings of the Royal Society of London Series A* 201 (1950) 40–61.
- [28] V. Freise, Zur theorie der diffusen doppelschicht, *Zeitschrift für Elektrochemie* 56 (1952) 822–827.
- [29] M. Eigen, E. Wicke, Zur theorie der starken elektrolyte, *Naturwissenschaften* 38 (1951) 453–454.
- [30] E. Wicke, M. Eigen, Über den einfluss des raumbedarfs von ionen in wässriger lösung auf ihre verteilung im elektrischen feld und ihre aktivitätskoeffizienten, *Zeitschrift für Elektrochemie* 56 (1952) 551–561.
- [31] M. Eigen, E. Wicke, The thermodynamics of electrolytes at higher concentrations, *Journal of Physical Chemistry* 58 (1954) 702–714.
- [32] M. Manciu, E. Ruckenstein, Lattice site exclusion effect on the double layer interaction, *Langmuir* 18 (2002) 5178–5185.
- [33] I. Borukhov, Charge renormalization of cylinders and spheres: ion size effect, *Journal of Polymer Science Part B: Polymer Physics* 42 (2004) 3598.
- [34] E. Trizac, J.L. Raimbault, Long-range electrostatic interactions between like-charged colloids: steric and confinement effects, *Physical Review E* 60 (1999) 6530–6533.
- [35] G. Barbero, L.R. Evangelista, D. Olivero, Asymmetric ionic adsorption and cell polarization in liquid crystals, *Journal of Applied Physics* 87 (2000) 2646–2648.
- [36] L. Lue, N. Zoeller, D. Blankschtein, Incorporation of nonelectrostatic interactions in the Poisson–Boltzmann equation, *Langmuir* 15 (1999) 3726–3730.
- [37] S. Lamperski, C.W. Outhwaite, Exclusion volume term in the inhomogeneous Poisson–Boltzmann theory for high surface charge, *Langmuir* 18 (2002) 3423–3424.
- [38] I. Bivas, Y.A. Ermakov, Elasticity and electrostatics of amphiphilic layers, *Advances in Planar Lipid Bilayers and Liposomes* 5 (2007) 313–343.
- [39] A. Silalahi, A. Boschitsch, R. Harris, M. Fenley, Comparing the predictions of the nonlinear Poisson–Boltzmann equation and the ion size-modified Poisson–Boltzmann equation for a low-dielectric charged spherical cavity in an aqueous salt solution, *Journal of Chemical Theory and Computation* 6 (12) (2010) 3631–3639.
- [40] D.W.R. Gruen, S. Marčelja, Spatially varying polarization in water, *Journal of the Chemical Society, Faraday Transactions II* (79) (1983) 225–242.
- [41] J.J. Lopez-García, J. Horno, C. Grosse, Poisson–Boltzmann description of the electrical double layer including ion size effects, *Langmuir* 27 (23) (2011) 13970–13974.
- [42] E. Gongadze, U. van Rienen, V. Kralj-Iglič, A. Iglič, Langevin–Poisson–Boltzmann equation: point-like ions and water dipoles near a charged membrane surface, *General Physiology and Biophysics* 30 (2) (2011) 130–137.
- [43] A. Bandyopadhyay, S. Chakraborty, Combined effects of interfacial permittivity variations and finite ionic sizes on streaming potentials in nanochannels, *Langmuir* 28 (17552) (2012) 13970–13974.
- [44] I. Szalai, S. Nagy, S. Dietrich, Nonlinear dielectric effect of dipolar fluids, *Journal of Chemical Physics* 131 (2009) 154905.
- [45] I. Szalai, S. Dietrich, Magnetization and susceptibility of ferrofluids, *Journal of Physics: Condensed Matter* (2008) 204122.
- [46] E. Gongadze, A. Iglič, Decrease of permittivity of an electrolyte solution near a charged surface due to saturation and excluded volume effects, *Bioelectrochemistry* 87 (2012) 199–203.
- [47] E. Verwey, J. Overbeek, *Theory of the Stability of Lyophobic Colloids*, Elsevier Publishing Company Inc., Weinheim, 1948.
- [48] D.F. Evans, H. Wennerström, *The Colloidal Domain: Where Physics, Chemistry, Biology, and Technology Meet*, 2nd ed., Wiley-VCH, New York, 1999.
- [49] J. Urbanija, K. Bohinc, A. Bellen, S. Maset, A. Iglič, V. Kralj-Iglič, P.S. Kumar, Attraction between negatively charged surfaces mediated by spherical counterions with quadrupolar charge distribution, *Journal of Chemical Physics* 129 (2008) 105101.
- [50] Y. Kim, J. Yi, P. Pincus, Attractions between like-charged surfaces with dumbbell-shaped counterions, *Physical Review Letters* 101 (2008) 208305.
- [51] S. May, A. Iglič, J. Reščič, S. Maset, K. Bohinc, Bridging like-charged macroions through long divalent rod-like ions, *Journal of Physical Chemistry B* 112 (2008) 1685–1692.
- [52] V. Bloomfield, DNA condensation, *Current Opinion in Structural Biology* 6 (1996) 334–341.
- [53] J. Urbanija, N. Tomšič, M. Lokar, A. Ambrožič, S. Čučnik, B. Rozman, M. Kandušar, A. Iglič, V. Kralj-Iglič, Coalescence of phospholipid membranes as a possible origin of anticoagulant effect of serum proteins, *Chemistry and Physics of Lipids* 150 (2007) 49–57.
- [54] V. Šuštar, J. Zelko, P. Lopalco, S. Lobasso, A. Ota, N.P. Ulrih, A. Corcelli, V. Kralj-Iglič, Morphology, biophysical properties and protein-mediated fusion of archaeosomes, *PLoS ONE* 7 (2012) e39401.
- [55] V. Kralj-Iglič, Stability of membranous nanostructures: a possible key mechanism in cancer progression, *International Journal of Nanomedicine* 7 (2012) 3579–3596.

- [56] A. Grosberg, T. Nguyen, B. Shklovskii, The physics of charge inversion in chemical and biological systems, *Reviews of Modern Physics* 74 (2002) 329–345.
- [57] R. Netz, Electrostatics of counter-ions at and between planar charged walls: from Poisson–Boltzmann to the strong-coupling theory, *European Physical Journal E* 5 (2001) 557–574.
- [58] J. Zelko, A. Igljič, V. Kralj-Igljič, S.P.B. Kumar, Effects of counterion size on the attraction between similarly charged surfaces, *Journal of Chemical Physics* 133 (2010) 204901.
- [59] E. Gongadze, A. Velikonja, T. Slivnik, V. Kralj-Igljič, A. Igljič, The quadrupole moment of water molecules and the permittivity of water near a charged surface, *Electrochimica Acta* 109 (2013) 656–662.
- [60] H. Fröhlich, *Theory of Dielectrics*, Clarendon Press, 1964.
- [61] A. Velikonja, Š. Perutkova, E. Gongadze, P. Kramar, A. Polak, A. Maček-Lebar, A. Igljič, Monovalent ions and water dipoles in contact with dipolar zwitterionic lipid headgroups – theory and MD simulations, *International Journal of Molecular Sciences* 14 (2013) 2846–2861.
- [62] L. Onsager, Electric moments of molecules in liquids, *Journal of the American Chemical Society* 58 (1936) 1486.
- [63] A. Abrashkin, D. Andelman, H. Orland, Dipolar Poisson–Boltzmann equation: ions and dipoles close to charge interfaces, *Physical Review Letters* 99 (7) (2007) 077801.
- [64] A. Igljič, E. Gongadze, K. Bohinc, Excluded volume effect and orientational ordering near charged surface in solution of ions and Langevin dipoles, *Bioelectrochemistry* 79 (2010) 223–227.
- [65] A. Velikonja, P.B. Santhosh, E. Gongadze, M. Kulkarni, K. Eleršič, Š. Perutkova, V. Kralj-Igljič, N.P. Ulrih, A. Igljič, Interaction between charged or dipolar lipid headgroups and charged nanoparticles mediated by water dipoles and ions, *International Journal of Molecular Sciences* 14 (8) (2013) 15312–15329.
- [66] O. Teschke, G. Ceotto, E. de Souza, Interfacial aqueous solutions dielectric constant measurements using atomic force microscopy, *Chemical Physics Letters* 326 (2000) 328–334.
- [67] O. Teschke, G. Ceotto, E. de Souza, Interfacial water dielectric-permittivity-profile measurements using atomic force microscopy, *Physical Review E* 64 (2001) 011605.
- [68] E. Gongadze, D. Kabaso, S. Bauer, T. Slivnik, P. Schmuki, U. van Rienen, A. Igljič, Adhesion of osteoblasts to a nanorough titanium implant surface, *International Journal of Nanomedicine* 6 (2011) 1801–1816.
- [69] F. Wiegand, P. Strating, Distribution of electrolytes with excluded volume around a charged DNA molecule, *Modern Physics Letters B* 7 (1993) 483–490.
- [70] A. Igljič, V. Kralj-Igljič, Influence of finite size of ions on electrostatic properties of electric double layer, *Electrotechnical Review (Slovenia)* 61 (1994) 127–133.
- [71] V. Lockett, R. Sedev, J. Ralston, M. Horne, T. Rodopoulos, Differential capacitance of the electrical double layer in imidazolium based ionic liquids – influence of potential, cation size, and temperature, *Journal of Physical Chemistry C* 1124 (2008) 7486–7495.
- [72] V. Lockett, M. Horne, R. Sedev, T. Rodopoulos, J. Ralston, Differential capacitance of the double layer at the electrode/ionic liquids interface, *Physical Chemistry Chemical Physics* 12 (2010) 12499–12512.
- [73] M.V. Fedorov, N. Georgi, A.A. Kornyshev, Double layer in ionic liquids: the nature of the camel shape of capacitance, *Electrochemistry Communications* 12 (2010) 296–299.
- [74] M.V. Fedorov, A.A. Kornyshev, Towards understanding the structure and capacitance of electrical double layer in ionic liquids, *Electrochimica Acta* 53 (2008) 6835–6840.
- [75] K.B. Oldham, A Gouy–Chapman–Stern model of the double layer at a (metal)/(ionic liquid) interface, *Journal of Electroanalytical Chemistry* 613 (2008) 131–138.
- [76] A.A. Gurtovenko, I. Vattulainen, Effect of NaCl and KCl on phosphatidylcholine and phosphatidylethanolamine lipid membranes: insight from atomic-scale simulations for understanding salt-induced effects in the plasma membrane, *Journal of Physical Chemistry B* 112 (2008) 1953–1962.
- [77] M. Yi, H. Nymeyer, H.X. Zhou, Test of the Gouy–Chapman theory for a charged lipid membrane against explicit-solvent molecular dynamics simulations, *Physical Review Letters* 101 (2008) 038103.
- [78] S. Lee, S. Yuhua, N. Baker, Molecular dynamics simulations of asymmetric NaCl and KCl solutions separated by phosphatidylcholine bilayers: potential drops and structural changes induced by strong Na<sup>+</sup>-lipid interactions and finite size effects, *Biophysical Journal* 94 (2008) 3565–3576.
- [79] L. Kale, R. Skeel, M. Bhandarkar, R. Brunner, A. Gursoy, N. Krawetz, J. Phillips, A. Shinozaki, Greater scalability for parallel molecular dynamics, *Journal of Computational Physics* 151 (1999) 283–312.
- [80] J. Phillips, R. Braun, W. Wang, J. Gumbart, E. Tajkhorshid, E. Villa, C. Chipot, R. Skeel, L. Kale, K. Schulten, Scalable molecular dynamics with NAMD, *Journal of Combinatorial Chemistry* 26 (2005) 1781–1802.
- [81] T. Dardenn, D. York, L. Pedersen, Particle mesh Ewald: an  $n$ -log( $n$ ) method for Ewald sums in large systems, *Journal of Chemical Physics* 98 (1993) 10089.
- [82] U. Essmann, L. Perera, M. Berkowitz, The origin of the hydration interaction of lipid bilayers from MD simulation of dipalmitoylphosphatidylcholine membranes in gel and liquid crystalline phases, *Langmuir* 11 (1995) 4519–4531.
- [83] R. Vácha, S.W.I. Siu, M. Petrov, R.A. Böckmann, P.J.J. Barucha-Kraszewska, M. Hof, M. Berkowitz, P. Jungwirth, Effects of alkali cations and halide anions on the DOPC lipid membrane, *Journal of Physical Chemistry A* 113 (2009) 7235–7243.
- [84] R. Vácha, P. Jurkiewicz, M. Petrov, M. Berkowitz, R. Böckmann, J. Barucha-Kraszewska, M. Hof, P. Jungwirth, Mechanism of interaction of monovalent ions with phosphatidylcholine lipid membranes, *Journal of Physical Chemistry B* 114 (2010) 9504–9509.
- [85] P. Jurkiewicz, L. Cwiklik, A. Vojtišková, P. Jungwirth, M. Hof, Structure, dynamics, and hydration of POPC/POPS bilayers suspended in NaCl, KCl, and CsCl solutions, *Biochimica et Biophysica Acta* 1818 (2012) 609–616.
- [86] J. Urbanija, N. Tomšič, M. Lokar, A. Ambrožič, S. Čučnik, B. Rozman, M. Kandušar, A. Igljič, V. Kralj-Igljič, Coalescence of phospholipid membranes as a possible origin of anticoagulant effect of serum proteins, *Chemistry and Physics of Lipids* 150 (2007) 49–57.
- [87] E. Raspaud, M.O. de la Cruz, J. Sikorav, F. Livolant, Precipitation of DNA by polyamines: a polyelectrolyte behavior, *Biophysical Journal* 74 (1998) 381–393.
- [88] J. Sadar, D. Chan, Long-range electrostatic attractions between identically charged particles in confined geometries and the Poisson–Boltzmann theory, *Langmuir* 16 (2000) 324–331.
- [89] S. Carnie, S. McLaughlin, Large divalent cations and electrostatic potentials adjacent to membranes. A theoretical calculation, *International Journal of Molecular Sciences* 44 (1983) 325–332.
- [90] J. Kirkwood, J. Schumaker, Forces between protein molecules in solution arising from fluctuations in proton charge and configuration, *Proceedings of the National Academy of Science* 38 (1952) 863–871.
- [91] R. Kjellander, Ion-ion correlations and effective charges in electrolyte and macro-ion systems, *Berichte der Bunsen-Gesellschaft Physical Chemistry* 100 (1996) 894–904.
- [92] F. Oosawa, Interactions between parallel rodlike macro-ions, *Biopolymers* 6 (1968) 1633–1647.
- [93] F. Porcheron, B. Rousseau, M. Schoen, A. Fuchs, Structure and solvation forces in confined alkane films, *Physical Chemistry Chemical Physics* 3 (2001) 1155–1159.
- [94] A. Yodh, K.-H. Lin, J. Crocker, A.D. Dinsmore, R. Verma, P.D. Kaplan, Entropically driven self-assembly and interaction in suspension, *Philosophical Transactions: Mathematical, Physical and Engineering Sciences* 359 (2001) 921–937.
- [95] Y. Mao, M. Cates, H. Lekkerkerker, Depletion force in colloidal systems, *Physica A* 222 (1995) 10–24.
- [96] S. Asakura, F. Oosawa, On interaction between two bodies immersed in a solution of macromolecules, *Journal of Chemical Physics* 22 (1954) 1255–1256.
- [97] K. Bohinc, A. Igljič, S. May, Interaction between macroions mediated by divalent rod-like ions, *Europhysics Letters* 68 (2004) 494–500.
- [98] J. Jackson, *Classical Electrodynamics*, Wiley and Sons Inc., New York, 1999.
- [99] V. Perutková, M. Frank, K. Bohinc, K. Bobojevič, J. Zelko, B. Rozman, V. Kralj-Igljič, A. Igljič, Interaction between equally charged membrane surfaces mediated by positively and negatively charged nanoparticles, *Journal of Membrane Biology* 236 (2010) 43–53.
- [100] M. Hatlo, L. Lue, A field theory for ions near charged surfaces valid from weak to strong couplings, *Soft Matter* 5 (2009) 125–133.
- [101] A.G. Moreira, R.R. Netz, Simulations of counterions at charged plates, *European Physical Journal E* 8 (2002) 33–58.
- [102] G. Tresselt, Generalized Poisson–Fermi formalism for investigating size correlation effects with multiple ions, *Physical Review E* 78 (2008) 061506.
- [103] L.B. Bhuiyan, C.W. Outhwaite, Comparison of exclusion volume corrections to the Poisson–Boltzmann equation for inhomogeneous electrolytes, *Journal of Colloid and Interface Science* 331 (2009) 543–547.
- [104] J. Ibarra-Armenta, A. Martín-Molina, M. Quesada-Pérez, Testing a modified model of the Poisson–Boltzmann theory that includes ion size effects through Monte Carlo simulations, *Physical Chemistry Chemical Physics* 11 (2009) 309–316.
- [105] D. Frenkel, B. Smith, *Understanding Molecular Simulation*, Academic press, San Diego, 1996.
- [106] J. Lekner, Summation of Coulomb fields in computer-simulated disordered systems, *Physica A* 176 (1991) 485–498.
- [107] R. Sperb, An alternative to Ewald sums part I: Identities for sums, *Molecular Simulation* 20 (1998) 179–200.
- [108] P. Ewald, Evaluation of optical and electrostatics lattice potentials, *Annalen der Physik (Leipzig)* 64 (1921) 253–287.
- [109] V. Kralj-Igljič, V. Heinrich, S. Svetina, B. Žekš, Free energy of closed membrane with anisotropic inclusions, *European Physical Journal B* 10 (1999) 5–8.
- [110] V. Kralj-Igljič, B. Babnik, D.R. Gauger, S. May, A. Igljič, Quadrupolar ordering of phospholipid molecules in narrow necks of phospholipid vesicles, *Journal of Statistical Physics* 125 (2006) 727–752.
- [111] J. Jorgačevski, N.V.M. Fošnaric, M. Stenovc, M. Potokar, M. Kreft, V. Kralj-Igljič, A. Igljič, R. Zorec, Fusion pore stability of peptidergic vesicles, *Molecular Membrane Biology* 27 (2010) 65–80.
- [112] Š. Perutkova, M. Frank-Bertoncelj, B. Rozman, M. Fošnaric, V. Kralj-Igljič, A. Igljič, Influence of ionic strength on agglutination of like-charged phospholipid membranes induced by beta2-glycoprotein I – Experimental and theoretical study, *Colloids and Surfaces B* 111 (2013) 699–706.